Moss kill dates and modeled summer temperature track episodic snowline lowering and ice cap expansion in Arctic Canada through the Common Era

Gifford H. Miller[1,2], **Simon L. Pendleton**[3], **Alexandra Jahn**[1,4], **Yafang Zhong**[5], **John T. Andrews**[1], **Scott J. Lehman**[1], **Jason P. Briner**[6], **Jonathan H. Raberg**[1,2], **Helga Bueltmann**[7], **Martha Raynolds**[8], **Áslaug Geirsdóttir**[9], and **John R. Southon**[10]

[1]Institute of Arctic and Alpine Research, University of Colorado Boulder, Boulder, CO 80303, USA
[2]Department of Geological Sciences, University of Colorado Boulder, Boulder, CO 80303, USA
[3]Environmental Science and Policy Program, Plymouth State University, Plymouth, NH 03264, USA
[4]Department of Atmospheric and Oceanic Sciences, University of Colorado Boulder, Boulder, CO 80303, USA
[5]Space Science & Engineering Center, University of Wisconsin-Madison, Madison, WI 53706, USA
[6]Department of Geology, University at Buffalo, Buffalo, NY, USA
[7]Institute of Biology and Biotechnology of Plants, University of Münster, Münster, Germany
[8]Institute of Arctic Biology, University of Alaska Fairbanks, Fairbanks, AK, USA CE1
[9]Institute of Earth Sciences and Department of Earth Sciences, University of Iceland, Reykjavik 101, Iceland
[10]W.M. Keck Carbon Cycle AMS Laboratory, University of California at Irvine, Irvine, CA, USA CE2

Correspondence: Gifford H. Miller (gmiller@colorado.edu)

Abstract. TS1 Most extant ice caps mantling low-relief Arctic Canada landscapes remained cold based throughout the late Holocene, preserving in situ bryophytes killed as ice expanded across vegetated landscapes. After reaching peak late Holocene dimensions ~ 1900 CE, ice caps receded as Arctic summers warmed, exposing entombed vegetation. The calibrated radiocarbon ages of entombed moss collected near ice cap margins (kill dates) define when ice advanced across the site, killing the moss, and remained over the site until the year of their collection. In an earlier study, we reported 94 last millennium radiocarbon dates on in situ dead moss collected at ice cap margins across Baffin Island, Arctic Canada. Tight clustering of those ages indicated an abrupt onset of the Little Ice Age at ~ 1240 CE and further expansion at ~ 1480 CE coincident with episodes of major explosive volcanism. Here we test the confidence in kill dates as reliable predictors of expanding ice caps by resampling two previously densely sampled ice complexes ~ 15 years later after ~ 250 m of ice recession. The probability density functions (PDFs) of the more recent series of ages match PDFs of the earlier series but with a larger fraction of early Common Era ages. Post 2005 CE ice recession has exposed relict ice caps that grew during earlier Common Era advances and were preserved beneath later ice cap growth. We compare the 107 kill dates from the two ice complexes with 79 kill dates from 62 other ice caps within 250 km of the two densely sampled ice complexes. The PDFs of kill dates from the 62 other ice caps cluster in the same time windows as those from the two ice complexes alone, with the PDF of all 186 kill dates documenting episodes of widespread ice expansion restricted almost exclusively to 250–450 CE, 850–1000 CE, and a dense early Little Ice Age cluster with peaks at ~ 1240 and ~ 1480 CE. Ice continued to expand after 1480 CE, reaching maximum dimensions at ~ 1880 CE that are still visible as zones of sparse vegetation cover in remotely sensed imagery. Intervals of widespread ice cap expansion coincide with persistent decreases in mean summer surface air temperature for the region in a Community Earth System Model (CESM) fully coupled Common Era simulation, suggesting the primary forcings of the observed snowline lowering were both

modest declines in summer insolation and cooling resulting from explosive volcanism, most likely intensified by positive feedbacks from increased snow cover and sea ice and reduced northward heat transport by the oceans. The clusters of ice cap expansion defined by moss kill dates are mirrored in an annually resolved Common Era record of ice cap dimensions in Iceland, suggesting this is a circum-North-Atlantic–Arctic climate signal for the Common Era. During the coldest century of the Common Era, 1780–1880 CE, ice caps mantled $> 11\,000\,km^2$ of north-central Baffin Island, whereas $< 100\,km^2$ is glaciated at present. The peak Little Ice Age state approached conditions expected during the inception phase of an ice age and was only reversed after 1880 CE by anthropogenic alterations of the planetary energy balance.

1 Introduction

The Canadian Arctic Archipelago (CAA) supports nearly $150\,000\,km^2$ of glaciers and independent ice caps, the greatest concentration of land ice outside Greenland and Antarctica (Medrzycka et al., 2022 TS2). As Earth warms, regardless of forcing mechanism, strong positive feedbacks in the Arctic result in greater temperature increases there relative to the planetary average on all timescales (Miller et al., 2010). Consistent with this, the rate of contemporary warming for the Arctic is greater than for most other geographic regions (Rantanen et al., 2022), particularly across the North Atlantic sector (Zhong et al., 2018). All CAA glaciers are now losing mass as summers continue to warm (Gardner et al., 2012; Lenaerts et al., 2013; Noël et al., 2018). In a review of controls on glacier mass balance in the CAA, Koerner (2005) demonstrated that summer temperature explains $\sim 95\,\%$ of annual mass balance variations over the previous 40 years of record, with the winter mass balance having negligible explanatory power. Consequently, changes in glacier dimensions dominantly reflect changes in summer temperature, and changes in glacier dimensions over time provide one of the most reliable records for the evolution of past summer temperatures. Unlike biological proxies that require evaluating an organism's adaptions that mitigate climate stressors, glaciers have no strategy for survival. If it snows more in winter than it melts in summer, non-calving glaciers expand; conversely, if more mass is lost by summer melt than is gained through winter snowfall, they recede.

Baffin Island, the largest island in the CAA, is an elongate tilted Precambrian block, stretching $\sim 1600\,km$ parallel to the west coast of Greenland. The island was inundated by the Laurentide Ice Sheet (LIS) at the last glacial maximum. Although deglaciation proceeded rapidly under high summer insolation in the early Holocene, our field area (Fig. 1), remained beneath the residual ice sheet 7000 years ago, and it was probably not free of Laurentide ice until after 5 ka (Dyke, 2004). The Barnes Ice Cap, at the southern edge of our field area, is a remnant of the LIS, and the coastal highlands east of our field area never fully deglaciated in the Holocene (Pendleton et al., 2019a).

Our primary focus are the $30\,000\,km^2$ north-central uplands inscribed in Fig. 1, which rise gradually from sea level at the west coast to $\sim 900\,m$ a.s.l. inland, after which the land rises rapidly to the high-elevation, deeply dissected fiord country along the east coast, where the interfluves are mantled by large ice caps and cirque glaciers. In contrast, isolated small, thin ice caps currently cover $\sim 100\,km^2$ of the highest summits across the low-relief uplands. Vegetation is sparse, dominated by lichens and bryophytes, with less common vascular plants. The only woody plants are prostrate species of willow (*Salix*). Our sampled ice caps (Fig. 1) occur across a larger region of about $55\,000\,km^2$.

2 Neoglaciation

Although deglaciation of the Laurentide Ice Sheet from Baffin Island continued through most of the Holocene, the orbitally driven decline in Northern Hemisphere summer insolation after $\sim 11\,ka$ resulted in a gradual lowering of snowline and high-elevation ice cap expansion as early as 9 ka (Lecavalier et al., 2017; Pendleton et al., 2017). Local ice cap and cirque glaciers were advancing by 5 ka (Moore et al., 2001), considered the onset of Neoglaciation, with ice expansion widespread by $\sim 3\,ka$ (Miller, 1973). In response to the continuing decline in Northern Hemisphere summer insolation, Baffin Island ice caps reached their maximum dimensions during the Little Ice Age (1240–1900 CE), the coldest centuries of the Holocene (Miller et al., 2012). Initial dating of Neoglacial ice margins was by lichenometry (Miller, 1973; Locke and Locke, 1977 TS3; Davis, 1985 TS4) and subsequently based on cosmogenic isotopes in moraine boulders (Anderson et al., 2008; Briner et al., 2009; Crump et al., 2017). Continuous records of Neoglacial activity on Baffin Island are derived from lake sediment cores (Moore et al., 2001; Miller et al., 2005; Briner et al., 2006, 2016), all confirming maximum ice dimensions and/or summer cold during the Little Ice Age. Ives (1957, 1962) was the first to recognize that spectral differences in aerial imagery of northern Baffin Island indicated that sparsely vegetated regions reflected a Little Ice Age (LIA) lowering of the snowline that killed all vegetation beneath the ice and that early 20th-century warming had reduced an extensive LIA ice complex to the few small remaining ice caps that mantle the highest summits (Williams, 1978). Wolken et al. (2005) evaluated the evidence for and against permanent ice cover explaining the sparsely vegetated zones, concluding that permanent ice cover was indeed the most likely cause. Although revegetation is rapidly occurring, the spectral signal remains preserved in recent satellite imagery (Fig. 2), although it is less distinct than in imagery from the 1950s. Andrews et al. (1975 TS5, 1976) used the light-toned areas on air photos

Figure 1. Field area, northern Baffin Island. The solid line defines regions for which the area–elevation relation is quantified in Fig. S1 and used to reconstruct the area covered by descending snow lines (Fig. 16) and the area of limited vegetation cover that defines ice cap outlines at the peak cold of the Little Ice Age. The dotted white square is the area covered by Fig. 2. Encircled dots show locations of all 186 moss kill dates (some dots include multiple samples). A portion of the Barnes Ice Cap is in lower-right corner. The inset in the upper right shows Baffin Island and the location of this image. Basemap © Google Earth.

and satellite imagery to produce the first map of perennial ice cover over north-central Baffin Island at the peak of the Little Ice Age. However, dating of the LIA snowline minimum remained uncertain.

5 Falconer (1966) TS7 was the first to recognize that the receding upland ice caps were frozen to their beds. Rather than active erosive agents, they are exceptional preservation agents. Bedrock striae appearing as contemporary ice recedes show ice flow to the NE around all margins of current ice 10 caps, reflecting only regional Laurentide Ice Sheet flow at the Last Glacial Maximum (LGM; Dyke, 2004). Striae, relict patterned ground (Falconer, 1966), delicately perched LGM erratic boulders resting on NE-trending striae appearing as contemporary ice surfaces lower (Fig. 3) and the lack of 15 englacial debris confirm cold-based ice. As ice caps recede, they also reveal entombed vegetation in positions of growth. The calibrated radiocarbon ages of dead moss ("kill dates") define when ice expanded across the site, killing vegetation, and then remained over the site, preserving the dead plants

until ice recession. Once exposed, dead vegetation is effi- 20 ciently removed by meltwater or wind-blown snow within a few years, although in rare settings devoid of meltwater, ice-killed vegetation is known to survive intact for several decades (e.g., Miller et al., 2017; Pendleton et al., 2017). Falconer (1966) reported the first radiocarbon date on in situ 25 dead moss collected at the margin of Tiger Ice Cap (Fig. 2), 330 ± 75 yr BP (I-1204), confirming ice expansion occurred during the Little Ice Age, but the precision is too low to include here. Miller visited the same ice cap in 1981, collecting moss at the ice edge that returned a ^{14}C age of 460 ± 25 30 (GSC-5025), early in the Little Ice Age.

Here we report 186 calibrated radiocarbon dates on in situ dead moss collected at the margins of receding ice caps that mantle summits across the uplands of northern Baffin Island, including all 107 ice-marginal dates within the area 35 inscribed in Fig. 1 and an additional 79 Common Era dates from 62 other local glaciers and ice caps in the adjacent high-elevation mountainous regions (Fig. 1). We report kill dates
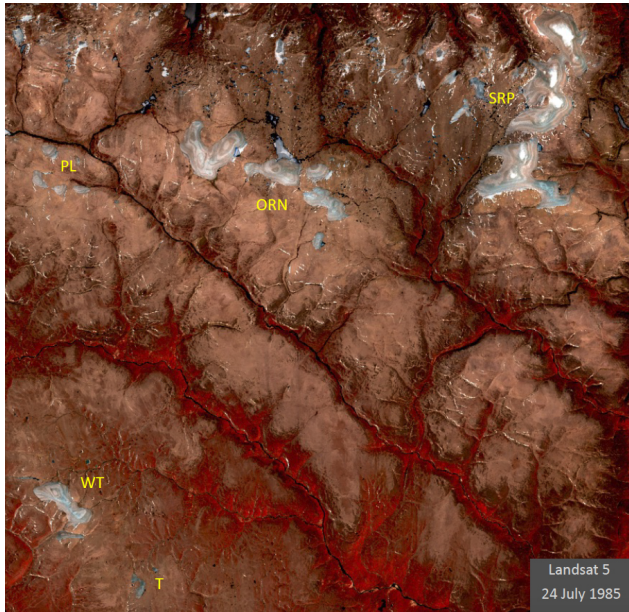
Figure 2. A 1985 Landsat 5 CIR image that has been color enhanced to maximize the spectral contrast that highlights lighter-toned regions that are sparsely vegetated. Those regions were beneath ice caps for at least several decades during the peak summer cold of the Little Ice Age. Labels are for the Serpens (SRP) and Orion (ORN) ice cap complexes, White Tiger (WT) and Tiger (T) ice caps, and Pleiades ice cap cluster (PL). The location of image is shown with a dashed line in Fig. 1.

from two densely sampled ice cap complexes, each sampled ~ 15 years apart, and compare those ages with Common Era dates from 62 other ice caps within 250 km of the densely sampled ice complexes. Three age clusters defined by the probability density functions (PDFs) of the composited 186 kill dates are compared with mean summer temperatures simulated in a fully coupled climate model for the Common Era (CESM past2k; Zhong et al., 2018). The kill date clusters correspond to century-scale anomalously cold summers in the model, whereas gaps between kill date clusters are relatively warm summers in the model. The close correspondence between modeled summer temperatures and changes in ice cap dimensions allows us to constrain the age of previously undated, low-elevation, sparsely vegetated zones that define an interval of extensive ice cap cover at elevations up to 400 m below extant ice cap margins.

3 Methods

Beginning in 2005, we built on the pioneering work of Ives, Andrews and Falconer[TS8], collecting in situ dead moss, usually within a meter of the ice margin at the time of collection. We concentrated our field studies on the low-relief upland of north-central Baffin Island between the Barnes Ice Cap and Lancaster Sound (Fig. 1), with permission from the Qikiq-

Figure 3. Delicately perched boulder left by the receding the Laurentide Ice Sheet that has recently emerged by the down-wasting of the local ice cap in the background. Striae on the underlying bedrock are toward the NE, in line with the flow of regional Laurentide ice in this area at the LGM. The preservation of such delicate features demonstrates the lack of internal deformation in cold-based ice caps that mantle the low-relief hills of the Baffin Island uplands. Photo by Gifford H. Miller.

tani Inuit licensed through the Nunavut Research Institute. We densely sampled two ice complexes mantling the highest uplands: the Serpens Ice Complex (SRP), consisting of three primary ice caps, and the Orion Ice Complex (ORN; both unofficial names), consisting of six ice caps in 2005 (Fig. 2). Additional collections were made in 2009, 2010, 2018 and 2019.

3.1 Radiocarbon-dated moss

Our primary data set is the radiocarbon ages of in situ ice edge dead moss. Ice margin retreat rates were measured at $\sim$ 10 m yr^{-1}, and vertical lowering was measured at ≥ 1 m yr^{-1} (2006–2008 CE), confirming vegetation collected a few meters from the ice margin was exposed during the year of collection. Regions where similar studies use moss kill dates to reconstruct the timing of Neoglacial ice cap expansion include Franz Josef Land (Lubinski et al., 1999[TS9]), Svalbard (Miller et al., 2017), Greenland (Lowell et al., 2013; Medford et al., 2021; Schweinsberg et al., 2017, 2018; Søndergaard et al., 2019), Baffin Island (Falconer, 1966; Anderson et al., 2008; Miller et al., 2013; Margreth et al., 2014; Pendleton et al.[TS10], 2019a, b), Alaska (Calkin and Ellis, 1981), Iceland (Harning et al., 2016), and Antarctica (Yu et al., 2016[TS11]; Groff et al., 2023).

We target members of the widespread moss family Polytrichaceae, primarily the genus *Polytrichum*, which has a thickened central stem of sufficient mass such that a single stem is adequate for a precise AMS[CE3] ^{14}C date. We previously showed that the ^{14}C concentration in living *Poly-*
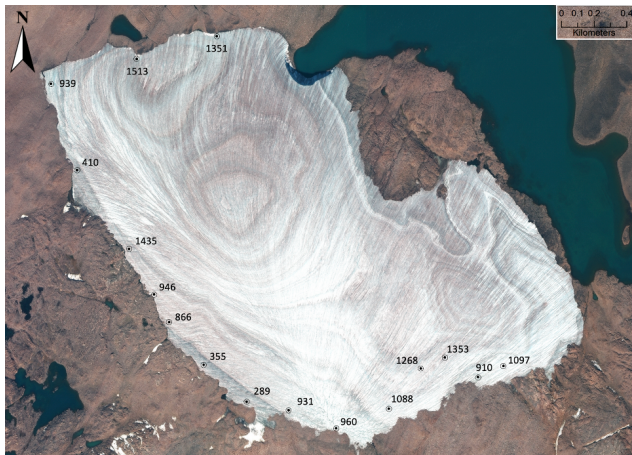
Figure 4. Vertical image of one ice cap in the Orion Ice Complex (~ 4 km long axis) captured on 20 August 2015, with median calibrated kill dates (CE year) for dead moss located at their ice edge coordinates when collected in 2018. The three early Common Era kill dates (289, 355, 410 CE) are situated beneath ice with distinctive surface characteristics that differ from the rest of the ice cap, consistent with them being a remnant early Common Era ice cap that expanded, killing the moss, followed by partial retreat, and subsequently subsumed by a late first millennium CE episode of ice cap growth, as well as later Little Ice Age ice cap growth, with dead moss now being revealed as ice is melting at all elevations. These small ice caps on nearly flat landscapes do not expand and recede symmetrically; they are frozen to their beds and exhibit little internal ice flow. Imagery © 2020 Maxar.

trichum is in equilibrium with that of the contemporary atmosphere, that ^{14}C dates on different *Polytrichum* stems in a single clump are statistically indistinguishable, confirming that they grow relatively quickly, and that ^{14}C dates on
5 *Polytrichum* collected at four sites along 200 m of a modern ice cap margin are statistically indistinguishable (Fig. S1 in the Supplement). These data sets support the interpretation that the timing of ice cap expansion can be reliably reconstructed from the ^{14}C kill dates on in situ dead *Polytrichum*
10 and other mosses revealed as ice caps recede under contemporary warming. We note, however, that very different kill dates can occur over ice margin distances of a few tens of meters, when the receding ice margin intercepts a buried, older ice cap preserved beneath a more recent ice expansion
15 (Fig. 4).

Although *Polytrichum* is the most common moss appearing as ice margins recede, if *Polytrichum* is not present, we rely on *Andreaea*, a genus of small rock mosses that commonly grow on siliceous rocks; they represent 9 % of
20 the dated samples. Because they are small, multiple strands are required for dating. Another 30 % of the dated samples were collected before we assigned taxonomic names to moss collections; they are almost all likely to be Polytrichaceae. Radiocarbon dates on co-located lichens are al-
25 ways older and are not included here. In the lab, plant sam-

ples are sonicated in deionized water, then freeze-dried. From the freeze-dried samples, sufficient material (~ 2 mg) was separated and submitted for dating. Combustion and graphitization of cleaned CO_2 is accomplished in INSTAAR's Laboratory for AMS Radiocarbon Preparation and Research
30 (NSRL) and measured at the W. M. Keck Carbon Cycle Accelerator Mass Spectrometry Laboratory at the University of California, Irvine; a few samples were measured at the National Ocean Sciences Accelerator Mass Spectrometry at the Woods Hole Oceanographic Institution. Radio-
35 carbon dates were calibrated using OxCal 4.2.4 and IntCal20 (Bronk Ramsey, 2009 TS12; Reimer et al., 2020) and expressed in years CE ($\pm 2\sigma$. Some of our dates were reported previously using IntCal13, resulting in small changes in the calibrated age distributions in this paper. The OxCal
40 program reports the probability as a percentage for each year provided by the calibration process. For collections of interest we sum the yearly probabilities, and then we normalize and plot them as a probability density function (PDF). Samples from multiple years and from different regions can be
45 aggregated and effectively compared this way. A complete tabulation of sample details and calibrated ages for all 186 samples used in this report is available at the NSF Arctic Data Center (https://doi.org/10.18739/A2RN30884, Pendleton and Miller, 2023 TS13).
50

3.2 Climate modeling

We make use of the CESM1-CAM5 (Hurrell et al., 2013) "past2k" transient climate simulation of the Common Era (1–2005 CE; Zhong et al., 2018). This simulation has 2° resolution in the atmosphere and land and ~ 1° resolution in
55 the ocean and sea ice, the same configuration as used for the CESM Last Millennium Ensemble (LME; Otto-Bliesner et al., 2016). The past2k forcing data (Fig. 5) were mostly from the Paleoclimate Model Intercomparison Phase 4 project (PMIP4; Jungclaus et al., 2017) for the Coupled Model In-
60 tercomparison Project Phase 6. They include changes in solar irradiance and insolation, volcanic aerosols (Toohey et al., 2016 TS14), and greenhouse gas levels (MacFarling et al., 2006). The land cover forcing for the past2k simulation from 850 to 2005 CE is taken from the LME, which im-
65 plements changes in grassland and cropland as compiled by PMIP3. The land cover forcing from 1 to 849 CE is a superposition of HYDE3.1 cropland changes (Goldewijk et al., 2011) onto the land cover forcing from the LME for 850 CE (see Zhong et al., 2018, for full details).
70

For us to assess the importance of anthropogenic activities in terminating the Little Ice Age, we also use existing CESM1-CAM5 simulations at ~ 1° resolution in all model components for 1850–2005 CE. Specifically, we make use of the simulated summer temperatures from four simulations
75 with all forcings (Hurrell et al., 2013), the standard "historical" forcing used for the CESM1 CMIP5 simulations. We also use summer temperatures from three simulations with
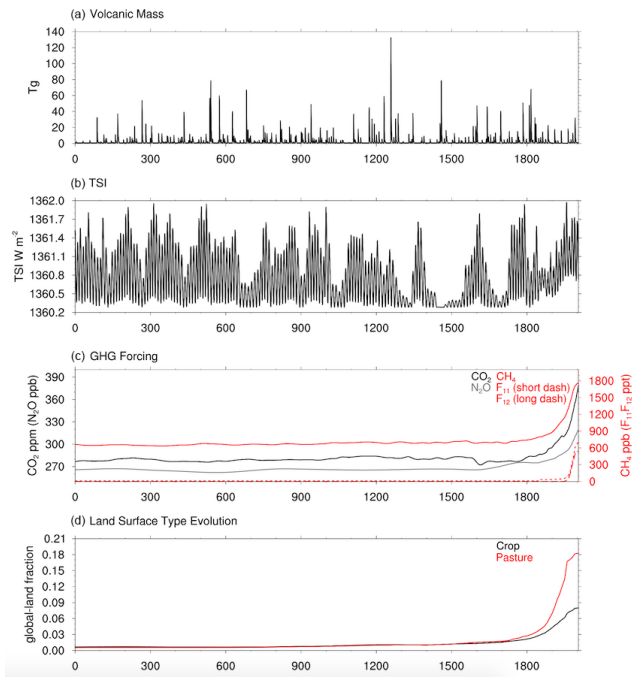
Figure 5. Forcing used for the past2k climate model discussed in the text. **(a)** Mass of sulfuric acid injected into the stratosphere by explosive volcanism in teragrams. **(b)** Total solar irradiance (TSI) in $\mathrm{W\,m^{-2}}$. **(c)** Concentrations of anthropogenic greenhouse gases released through the Common Era. **(d)** Anthropogenic changes in global land cover through the development of crops (upper line) and pastures (lower line) through the Common Era.

only "natural" forcings. The natural forcing experiment is forced only by solar variability and volcanic aerosol emissions, following the CMIP5 protocol (Taylor et al., 2012), and is part of a published data set of single forcing experiments with the CESM1-CAM for 1850–2005 that were previously used in other studies (Meehl et al., 2020; Taylor et al., 2012; Xu et al., 2022). By using all available ensemble members from these two experiments, we can assess the impact of the anthropogenic forcing beyond the influence of internal variability.

4   Results

4.1   Repeat sampling around the ORN and SRP ice complexes

In 2005 we collected dead moss around the margins of the Orion (ORN: 18 dated samples) and Serpens (SRP: 22 dated samples, 4 collected in 2009) ice complexes (Fig. 2). The composite PDF of both data sets showed similar kill date clusters (Miller et al., 2012). To test whether those clusters were artifacts of the state of the ice caps during the year of collection, we resampled ORN in 2018 and SRP in 2019,
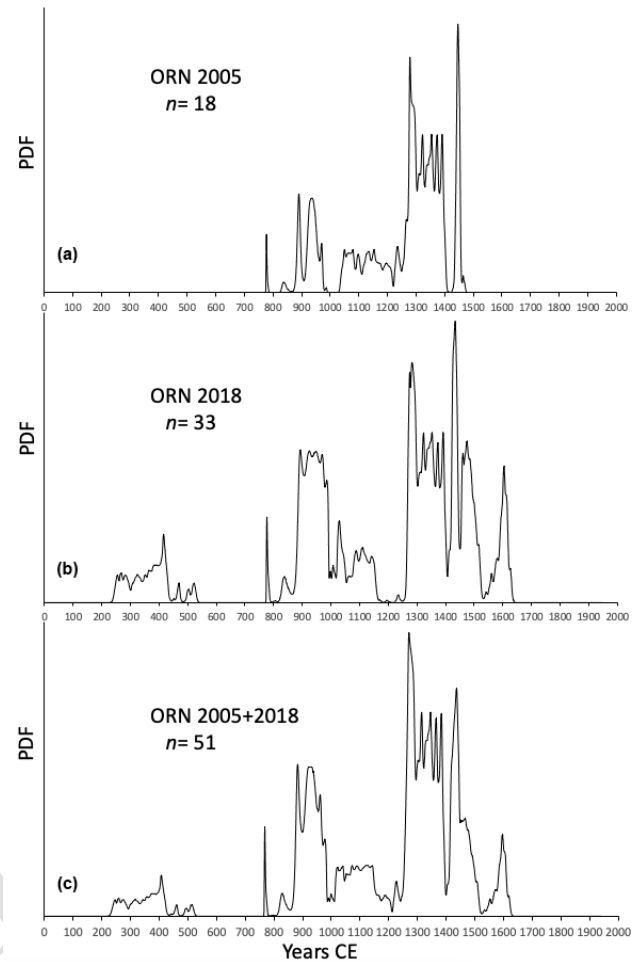

Figure 6. Probability density functions (PDFs) for calibrated radiocarbon dates on dead moss collected around the margins of the Orion Ice Complex (ORN, Fig. 2), which consists of several adjacent ice caps. **(a)** The PDF of 18 samples collected in 2005. **(b)** The PDF of 33 samples collected in 2018, which mirror the distribution from 2005, except for the addition of early first millennium CE samples in the latter group that reflect a buried ice cap now emerging from beneath a younger ice cap that overwhelmed (but did not incorporate) it (Fig. 4). **(c)** PDF of all dates from ORN from all years.

after $\sim 250\,\mathrm{m}$ of ice recession at both sites, with a greater sampling density.

4.1.1   Orion Ice Complex (Fig. 2)

The 2005 moss kill dates (Fig. 6a) cluster between 850 and 1000 CE and 1240 to 1480 CE, with a scattering of dates between the two clusters. The PDF of 33 kill dates collected in 2018 (Fig. 6b) is broadly similar, with dominant clusters between 850 and 1000 CE and between 1240 and 1500 CE but also an older cluster between 250 and 450 CE. In the 2005–2018 composite PDF (Fig. 6c) the older cluster reflects moss killed during an early first millennium CE expansion of ORN that likely melted partially after 450 CE but

never completely disappeared. The residual early first millennium CE ice cap was subsumed by a late first millennium CE expansion beginning ca. 850 CE and preserved beneath younger ice, only to re-emerge and restart recession under contemporary warming, exposing plants killed during the early first millennium CE ice expansion. For example, where ice-marginal moss produced early first millennium CE ages at one of the ORN ice caps, the ice surface characteristics visible in high-resolution imagery captured for us by Digital Globe differ in character from the glacier surface farther along the ice margin in either direction where the moss kill dates are much younger (Fig. 4), supporting our interpretation that in 2018 a remnant early first millennium CE ice cap that never melted completely was emerging from beneath a younger ice cap that grew when the snowline subsequently fell across the region. The near-identical alignment of the two younger 2018 clusters with those from 2005 confirms the utility of moss kill dates as reliable ages of Common Era ice cap expansion, regardless of collection date. A primary conclusion from these data is that summer temperatures over the past century are warmer, on average, than any century since 450 CE.

4.1.2   Serpens Ice Complex (Fig. 2)

The PDFs of the 2005 and 2009 (22 dates) and 2019 (34 dates) collections from SRP produce clusters in nearly identical time intervals from 250 to 450 CE, 850 to 1000 CE and 1240 to 1480 CE (Fig. 7).

4.1.3   The SRP + ORN PDF (Fig. 8)

The PDFs for all dates from SRP (Fig. 8a) and ORN (Fig. 8b) are combined as a SRP + ORN composite (Fig. 8c) consisting of 107 calibrated ^{14}C dates. That PDF has three well-defined clusters, reflecting an early first millennium CE expansion between 250 and 450 CE found in five samples from SRP and three from ORN. There is virtually no evidence of ice expansion between 450 and 850 CE, after which both ice complexes show expanding margins from 850 to 1000 CE (11 from ORN and 12 from SRP). ORN yielded six samples scattered between 1050 and 1160 CE but with no central tendency, whereas SRP has none. However, both SRP and ORN have large numbers of dates beginning ∼ 1240 CE and continuing until ∼ 1480 CE (25 from ORN and 37 from SRP), indicating ice margins expanded throughout that interval.

In both the SRP and ORN composite PDFs (Fig. 8c) the sharply defined peak centered on ∼ 780 CE is related to calibration. Radiocarbon ages between 1080 and 1180 yr BP have median calibrated ages between 850 and 960 CE, but they all also have a low (<∼ 5 %) probability of an age clustered tightly around 780 CE. Because 23 of the 109 radiocarbon dates from the two complexes are between 1080 and 1180 yr BP, their calibration creates a low-probability but strongly expressed peak clustered tightly around 780 CE. Be-
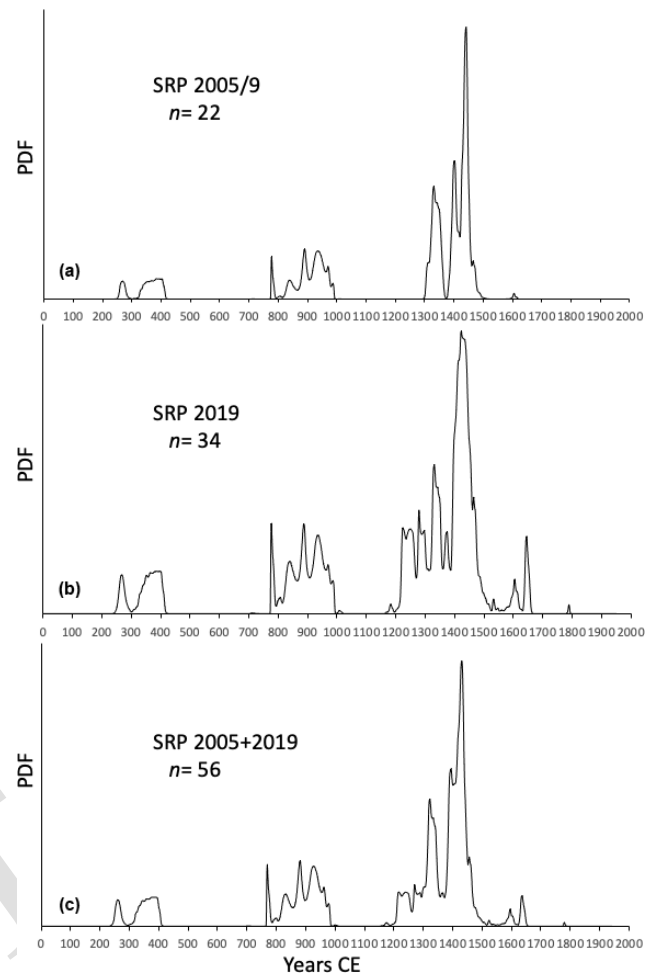

Figure 7. Probability density functions (PDF) for calibrated radiocarbon dates on dead moss collected around the margins of the Serpens Ice Complex (SRP, Fig. 2), which consists of three adjacent ice caps. **(a)** The PDF of 22 samples collected in 2005 and 3 others collected in 2009. **(b)** The PDF of 34 samples collected in 2019. **(c)** The composite PDF for all 56 kill dates from SRP form three discrete age clusters that exhibit little change between collection dates despite significant (∼ 250 m) ice margin recession.

cause of the low probability that this is the actual calibrated age, and lacking other samples in the same time range, we consider it highly unlikely that 780 CE is an interval of expanding ice caps.

We test the potential for variations in atmospheric ^{14}CO$_2$ concentrations to have influenced the structure of the SRP + ORN PDF (Fig. 8) by creating an artificial data set of 186 samples (one every 8 calendar years) spanning the 1500-year interval covered by our data set (1–1500 CE). We reverse calibrate those with the IntCal20 curve to derive a set of theoretical ^{14}C ages – what the ^{14}C ages "should be" – but we take into account the fact that the measured ^{14}C dates are not perfectly accurate by modifying with sigma equal to 18 years, the average of our dating precision for the moss
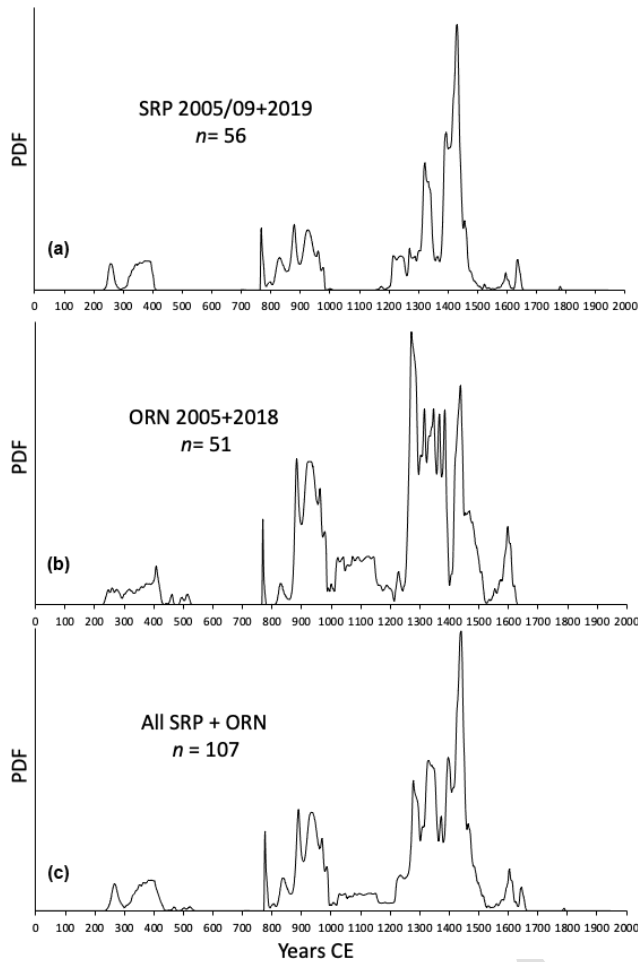
Figure 8. A comparison between probability density functions (PDF) for all calibrated radiocarbon dates on dead moss collected around the margins of ORN **(a)** and SRP **(b)** ice complexes (Fig. 2) showing the similarities between the two data sets. The composite PDF for the 107 moss kill dates from both ice complexes **(c)** defines tightly clustered episodes of ice cap expansion through the Common Era at 250–400 CE, 850–1000 CE, and between ~ 1240 and 1480 CE.

Figure 9. The composite PDF for calibrated ^{14}C ages of 186 calendar dates equally distributed between 1 and 1500 CE (dotted line) superposed on the same scale as the 186 calibrated kill dates to test whether changes in atmospheric $^{14}CO_2$ concentrations contributed to the clustering of kill dates in the SRP and ORN composite PDFs (Fig. 8). There is no strong correlation between the two PDFs, indicating any inherent calibration bias has no influence on the clustering of the moss kill dates.

ages. That modified set of simulated measured ^{14}C ages is calibrated using the IntCal20 curve, and the resulting probability distributions are summed to quantify calibration bias (Fig. 9), which has no pronounced peaks in the central clusters of kill dates shown in Fig. 8, supporting our contention that peaks in kill dates are a reliable estimate of expanding ice throughout the Common Era.

4.1.4 Testing the SRP + ORN composite (Fig. 10)

The combined SRP + ORN PDF defines sustained Common Era ice cap expansion limited to three primary intervals: 250 to 450 CE, 850 to 1000 CE and after 1240 CE. The SRP complex consists of three independent ice caps, whereas ORN consisted of six independent ice caps sampled in 2005, of
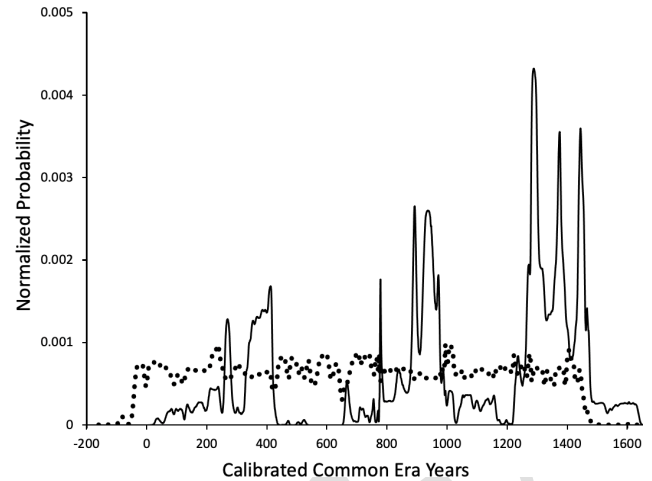
which portions of only three remain. To test whether the densely sampled ice complexes reflect the regional snowline lowering across northern Baffin Island, we collected 79 additional dead moss samples from the margins of 62 other ice caps. Those additional ice caps include other small ice caps situated on low-relief landscapes similar to ORN and SRP but also include low-relief summits within much larger ice complexes where ice expansion is primarily by vertical thickening rather than ice flow. None of the samples are from outlet glaciers; all are within 250 km of SRP and ORN. We avoid cirque glaciers because response times to snowline lowering are more complex than for small upland cold-based ice caps or the vertical thickening of large ice caps, both of which change in direct response to summer temperature and are largely unrelated to ice flow.

The resultant PDF of those 79 calibrated ages is compared with the PDF of the 107 dates from SRP + ORN in Fig. 10. The isolated ice cap dates (Fig. 10b) cluster primarily in the same three groupings apparent in the SRP + ORN PDF (Fig. 10a), although the early first millennium CE (250–450 CE) cluster is more strongly represented, and the onset extends to near the start of the first millennium CE. The three samples that contribute to that tail are from elevations above 900 m a.s.l., higher than ORN and SRP, suggesting that summer cooling began earlier than recorded by SRP + ORN and that snowline did not drop below 900 m a.s.l. until after 250 CE or that subsequent summer warmth fully melted all pre-CE advances. The 850–1000 CE cluster is apparent in both data sets, with similar overall structures, suggesting regional climate forcing. Both data sets lack signifi-
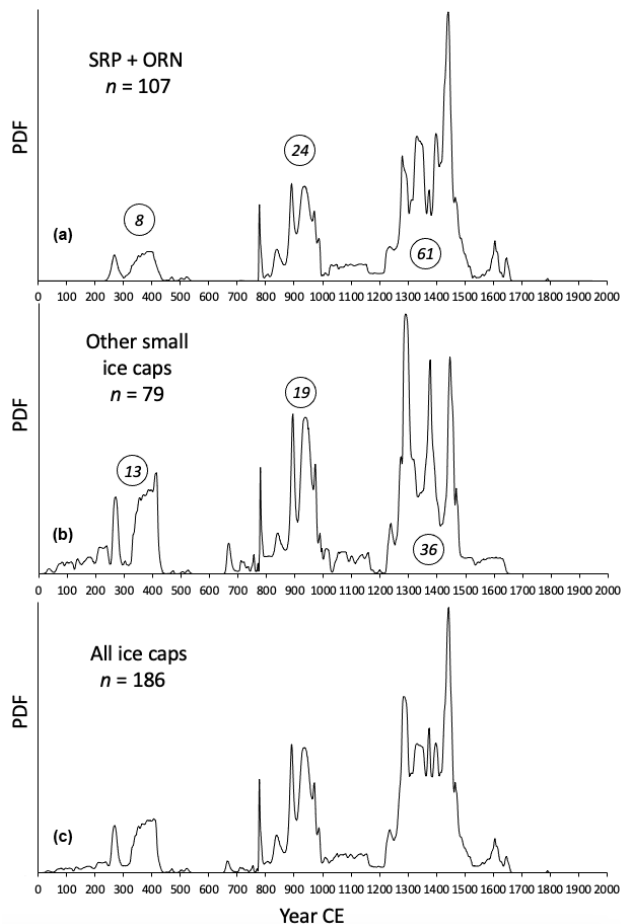
Figure 10. The PDF for all moss kill dates from SRP + ORN **(a)** and from the margins of all other small ice caps in Fig. 1 **(b)** are composited in panel **(c)**. Moss kill dates that make up panel **(b)** include all Common Era kill dates from 62 different ice caps (Fig. 1), all of which are within 250 km of the SRP and ORN ice complexes. The number of dates in each of the clusters is given as a circled number. The similarities between PDFs in panels **(a)** and **(b)** are striking, suggesting ice cap response to climate forcing over the Common Era was uniform across northern Baffin Island, lending confidence to a comparison of ice cap response and modeled climate forcing. Location data, lab IDs, ^{14}C ages and PDFs for each sample in panel **(c)** are available at the NSF Arctic Data Center (Pendleton and Miller, 2023). The spike at ∼ 780 CE is a very low probability calibration age CE4 in the calibration program.

cant ice expansion between 1000 and 1240 CE, and both exhibit evidence of widespread expansion beginning abruptly in ∼ 1240 CE and continuing to ∼ 1480 CE.

The large cluster of kill dates around 1240–1480 CE suggests snowline declined throughout that interval. However, at multiple sites ice edge moss collected in 2005 with kill dates of ∼ 1250 CE are older than ice edge moss sampled in 2018 from sites orthogonal to the 2005 ice margin, which show younger kill dates (∼ 1450 CE). The simplest explanation for this apparent contradiction is an interval of modest ice re-

cession after 1250 CE, followed by a readvance ∼ 1450 CE, with preservation of the older moss beyond the receded ice margin, which was re-covered during the ∼ 1450 CE expansion. This complex history of cold-based plateau ice caps advancing, receding and then re-advancing can be preserved in the ages of moss surviving multiple episodes of ice expansion. This is illustrated by the three early first millennium CE moss kill dates in Fig. 4 that are associated with ice of a different character than adjacent ice with much younger moss kill dates. This requires a remnant early first millennium CE ice cap to have been subsumed by an interval of late first millennium CE ice cap growth. We conclude from the positions of moss with kill dates between 1240 and 1480 CE that this 240-year interval was not characterized by monotonic summer cooling; instead summer cooling beginning in ∼ 1250 CE was interrupted by at least one episode of warm summers leading to modest ice recession followed by re-expansion of the ice caps in ∼ 1450 CE.

The composite record consisting of 186 calibrated radiocarbon dates from 70 different ice caps (Fig. 10c) constrains ice cap expansion during the Common Era across northern Baffin Island. The well-defined clusters suggest the snowline began to decline early in the first millennium CE, resulting in widespread ice cap expansion between 250 and 450 CE (21 dates). There is no evidence from kill dates for additional ice cap growth until after 800 CE, with widespread ice cap expansion between 850 and 1000 CE (43 dates). Although there is little evidence for snowline lowering during the medieval period, between 1000 and 1240 CE, summer temperatures were also not high enough to melt all ice caps that formed in the first millennium CE. This suggests that medieval times were certainly not as warm, on average, as the earliest centuries of the Common Era but also that medieval times experienced no sustained decades of significant summer cold. The year 1240 CE marks the start of the Little Ice Age, with clear evidence of intermittent ice cap expansion in all data sets continuing for the next 240 years (97 dates).

None of the kill dates from plateau ice caps pre-date the Common Era. Consequently, if earlier late Holocene episodes of summer cold resulted in long-lived ice caps across Baffin Island uplands, subsequent summers were warm enough and/or long enough to completely melt those ice caps before 1 CE. Our moss dates are relatively silent about the state of the ice caps after ∼ 1500 CE. We turn to climate models to derive information on ice cap dimensions after 1500 CE.

4.2 Modeling the evolution of Common Era summer temperature

From the past2k model output we extract simulated summer (June, July, August, JJA) 2 m air temperature averaged over North Atlantic Arctic land areas (> 60° N and between 90° W and 30° E) through the Common Era (1–2005 CE), capturing a broad representation of North Atlantic Arctic
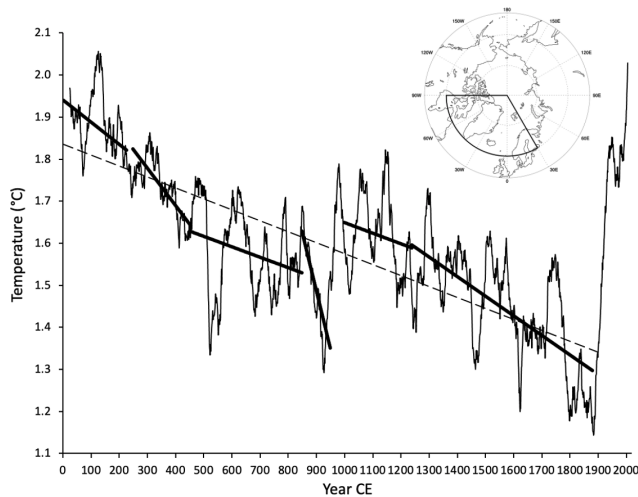
Figure 11. The 50-year running mean of modeled annual summer (JJA) temperature over land areas north of 60° N and between 30 and 90° W (shown in inset) between 1 and 2005 CE in our CESM past2k simulation. The dashed black line is a least-squares linear regression for the data between 1 and 1890 CE, showing a first-order trend of declining summer temperature through the Common Era. Solid lines are least-squares linear regressions through times defined by clusters of kill dates and the times between kill date clusters in Fig. 10c. The regressions allow a direct comparison of summer temperature trends and relative magnitudes for intervals characterized by widespread ice cap expansion (predicted cold summers) and intervals lacking evidence of sustained ice cap expansion (predicted mild summers). The time intervals defined by these trends can be compared to the reconstructed snowline elevations through the Common Era (Fig. 16).
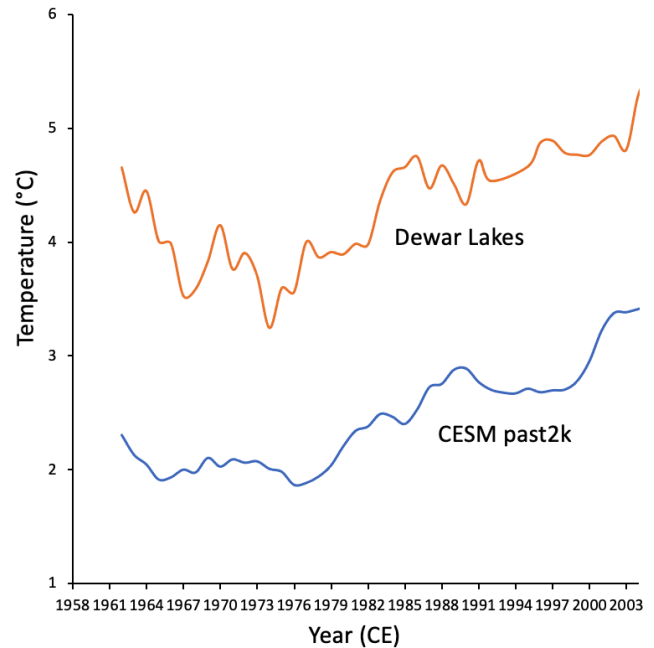
Figure 12. The 10-year running mean for JJA temperature measured daily at Dewar Lakes since 1958 (upper line) and 5-year running means of simulated JJA 2 m temperature over land north of 60° N and between 30° E and 90° W in our CESM past2k model run (lower line). Dewar Lakes temperatures are more strongly smoothed because site-specific records have greater variability than past2k, which is averaged over a large area that naturally smooths the data. The similarity in the patterns and magnitude of temperature change between model and data indicates that the past2k model reliably simulates the primary signal of summer temperatures across our field area through the Common Era.

lands and including the climate impacts from sea ice feedbacks. Although climate is often approximated using a 30-year average, cold-based ice caps mantling low-relief landscapes on Baffin Island have a longer, multidecadal response time, so we use a 50-year running mean for our data–model comparison. The 50-year running mean of summer temperature through the Common Era exhibits a first-order declining trend up to ∼ 1890 CE (Fig. 11), consistent with declining NH summer insolation from orbital terms. Because Baffin Island is only a portion of the land included in our extraction of mean JJA summer temperatures (Fig. 11 inset), the modeled temperatures are unlikely to match those of our field area, and we evaluate the relative changes in summer temperature without regard to absolute values.

To assess how well the past2k summer temperatures represent the summer temperature evolution in the study region, we compare the past2k summer temperatures with a 50-year record of summer temperature from the only Baffin Island interior weather station, Dewar Lakes, ∼ 350 km SE of our field area, at 500 m a.s.l. The mean summer (JJA) temperature at Dewar Lakes from 1958 to 2022 exhibits high inter-annual variability (up to 5 °C) and a range of al-

most 9 °C, but the 10-year running mean (Fig. 12) shows that relatively warm summers in the 1950s were followed by colder summers in the 1960s and early 1970s, after which variably warming summers dominate the record. The 5-year running mean for the summer temperature record in our CESM past2k simulation for the period of overlap (1958–2005; Fig. 12) reasonably mimics the Dewar Lakes record, when accounting for the expected much lower variability in the model results due to the averaging over a much larger area.

Both the Dewar Lakes recorded summer temperatures and CESM simulated summer temperatures indicate cold summers in the 1960s and early 1970s. We compare those records with ice cap retreat rates for three ice caps (WT, SRP, ORN; see Fig. 2) from remote images spanning 1957–2020 CE. All three ice caps show reduced rates of aerial decrease between 1960 and the early 1970s (Fig. 13), lending additional confidence to the simulated summer temperatures in the past2k results. Summer warming in both Dewar Lakes and past2k records since 1980 is matched by increased ice cap recession rates. The close correspondence between past2k mod-
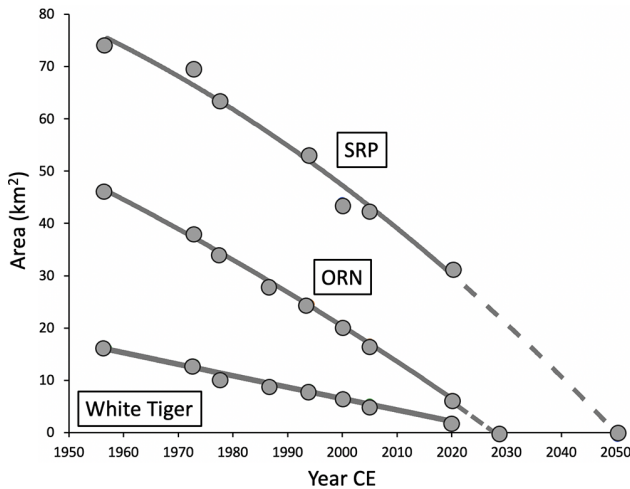
Figure 13. The change in area for three caps between 1957 and 2020 (Fig. 2): Serpens Ice Complex (SRP; three ice caps), Orion Ice Complex (ORN; six ice caps, four remaining in 2020 CE), and White Tiger (WT, one ice cap). All three show decreased recession rates between 1957 and 1972 CE, consistent with cold summers recorded at Dewar Lakes over the decade between 1958 and the mid-1970s CE, followed by steady, or increasing rates of mass loss after 1972. Areas are derived from vertical aerial photography from 1957 CE and satellite imagery subsequently. Updated from Anderson et al. (2008).

eled summer temperatures the Dewar Lakes recorded temperatures and rates of ice cap recession for WT, SRP and ORN provide a measure of confidence in the CESM modeled summer temperatures through the Common Era.

4.3   Comparing modeled summer temperatures with ice cap kill dates

Because summer temperature is the dominant control on Baffin Island glacier mass balance (Koerner, 2005), we expect below-average modeled summer temperatures to correspond with episodes of ice cap expansion. The modeled 50-year mean summer temperatures (Fig. 11) contain significant centennial-scale structures. Primary forcings (Fig. 4) leading to the temperature decline in the model include a reduction in Northern Hemisphere summer insolation through the Common Era; small reductions in TSI between 1300 and 1700 CE; and episodes of sulfur-rich explosive volcanism with the associated positive feedbacks from expanded sea ice, additional snow cover over land, and changes in ocean circulation. Anthropogenic impacts become important after $\sim$ 1850 CE.

A piecewise regression of JJA temperatures (1–1900 CE; Fig. S2) suggests an initial steep decline from 1 to 900 CE, followed by warming from 900 to 1050 CE, and finally a slower decline between 1050 and 1900 CE. While the piecewise regression captures some of the Common Era structure,

it lacks the detail necessary to compare with the kill date composite PDF (Fig. 10c).

To more directly compare past2k 50-year mean summer temperatures with the information provided by our moss kill dates, we instead calculate multi-century linear regressions of modeled summer temperature across time periods that kill dates indicate involved widespread ice cap expansion and across intervals lacking evidence of expanding ice caps (Fig. 11). This relaxes the constraints for piecewise regressions that require individual regressions to be continuous. The regression through mean summer temperatures between 250 and 450 CE defines a steady decline in summer temperature that accounts for $\sim$ 25 % of the modeled temperature decline between 1 and $\sim$ 1880 CE. The modeled summer temperature decline is consistent with the earliest kill date cluster centered on 250–450 CE (Fig. 10c). The modest number of kill dates between 1 and 250 CE (Fig. 10c) is consistent with the onset of cooling summers of 1 to 250 CE in the model, prior to the main cluster of kill dates beginning at 250 CE.

Declining summer temperatures from 250 to 450 CE were followed in the model by 50 years of warmth before a 50-year strongly negative temperature excursion resulting from 536 CE explosive volcanism (Büntgen et al., 2016) and associated positive feedbacks. A record of ice cap expansion at that time is not present in our kill dates. We presume the snowline dropped and ice caps grew at this time, but the short duration and rapid return to a century of relative warmth after the eruption likely resulted in enough melt that evidence of 536 CE ice cap expansion is lost.

High multidecadal temperature variability without a trend between 450 and 800 CE is predicted to result in changes in snowline, but because cold summers are brief (2 to 3 decades) and followed by warm summers, development of persistent ice caps is unlikely; hence, there are no kill dates. However, a strong 100-year cooling trend between 840 and 940 CE produced the coldest sustained temperatures of the first millennium CE and aligns with the second main kill date cluster between 850 and 1000 CE.

Modeled medieval temperatures in our past2k simulation suggest high-magnitude multidecadal variability between 950 and 1200 CE but without a trend and at a mean temperature similar to the coldest decades around 400 CE. This is consistent with medieval times not being warm enough to fully melt ice caps that formed early in the first millennium CE. However, the mean medieval summer temperature is warmer than summers during the 850–1000 CE ice expansion, in conflict with the 42 sites with kill dates between 850 and 1000 CE that remained intact through the medieval period. We suggest that either the late first millennium CE summer temperatures are too low or modeled medieval summer warmth is too high to be reconciled with strong the cluster of dead vegetation ages of 850–1000 CE; an explanation for this discrepancy remains unresolved.

From 1240 to 1880 CE, summer temperatures decline overall in the model, consistent with our kill dates and with

the low snowline required by the elevations of sparsely vegetated lowlands (Fig. 2). Finding ~ 1240 CE kill dates outboard of 1480 CE dates (Sect. 4.1.4) requires a multidecadal oscillation of ice cap dimensions (e.g., a ~ 1240 CE advance, followed by ice recession without all dead moss eroded away, followed by a subsequent advance at ~ 1480 CE that allowed ice caps to re-cover moss killed in 1240 CE), and to also kill newly colonized moss both inboard and outboard of the 1240 CE sites. This is consistent with modeled summer temperatures exhibiting significant multidecadal variability but never warm enough or long enough to melt all ice that expanded at ~ 1240 CE, early in the Little Ice Age. The lack of kill dates younger than 1500 CE suggests it is unlikely there was any century after 1500 CE with average summer temperatures higher than the 1240–1480 CE mean until 20th-century warming, which is consistent with modeled summer temperatures (Fig. 11).

Modeled summer temperature decreases after medieval times are a response to major explosive volcanism at ~ 1240 and ~ 1440 CE (40 and 50 years, respectively; Sigl et al., 2015). A total of 18 of 186 kill dates (Fig. 10c) have median calibrated ages between 1440 and 1480 CE, suggesting widespread ice expansion then. The 97 sites with kill dates between 1240 and 1500 CE indicate expansion of ice caps across those two centuries, consistent with large sulfur-rich volcanic eruptions that produce a first-order declining trend in modeled summer temperatures.

There is broad agreement between modeled summer temperatures and the temporal distribution of kill dates, with the three primary clusters of kill dates centered on episodes of centennial-scale declines in past2k modeled summer temperatures. The cluster of kill dates between 1240 and 1480 CE aligns with the beginning of a 600-year irregular temperature decline in modeled summer temperature, culminating in the coldest century of the common era between 1780 and 1880 CE. Rapid warming in the past2k model after ~ 1880 CE is consistent with rapid cryosphere recession that reduced the ice-covered area across the north-central Baffin Island uplands from $\sim 11\,000$ km^2 at the LIA maximum to ~ 400 km^2 by 1960 CE and < 100 km^2 in 2022 CE.

5   Discussion

5.1   Age of maximum Common Era ice cap expansion

The swaths of sparsely vegetated regions across north-central Baffin Island first noted 70 years ago (Ives, 1957) define the lowest persistent snowline of the Common Era and represent the peak cold of the Little Ice Age (Ives, 1962; Andrews et al., 1975, 1976; Williams, 1978; Locke and Locke, 1977), but independent dating of that interval has been elusive. To kill all vegetation requires multidecadal burial beneath ice. Because the regions that define peak LIA snowline lowering are discontinuous (Fig. 2), more than 100 independent, cold-based ice caps, each a few tens of meters thick, and ranging from ~ 50 km^2 to a few hundred square kilometers in area must have mantled the currently sparsely vegetated uplands during a century or more of coldest LIA summers. The spectral character along the outer perimeters of the sparsely vegetated regions (Fig. 2) is mottled, suggesting a dominant "permanent" ice cap over higher hills and an outer perimeter where permanent snow lay in landscape hollows long enough to kill vegetation but not long enough to coalesce into the main ice cap.

Although sparsely vegetated landscapes define the maximum dimensions of ice caps in the Common Era, vegetation killed by that expansion was vulnerable to efficient removal by wind and water erosion as ice caps receded. In 2005 we visited a "sparsely vegetated" region apparent in remote imagery and found that revegetation was already advanced. We sampled a dead willow (*Salix*) stem at 629 m a.s.l., lower than any extant ice cap. The ^{14}C age of the stem is "modern" (CURL-7929: 1.16 FM), suggesting that vegetation killed by the lowest LIA snowline is rare or absent and little chance that radiocarbon can resolve when the snowline reached its maximum LIA dimensions.

Recession of ice caps from regions defined by vegetation contrasts was nearly complete by the middle of the 20th century when remotely sensed imagery first became available. Because the spectral contrast that defines the sparsely vegetated landscape in imagery from the 1950s is much stronger than in contemporary imagery due to ongoing revegetation and because the sparsely vegetated landscapes lack gradients in their spectral contrasts, ice recession from maximum LIA dimensions must have been relatively rapid and continuous.

The youngest kill dates are ~ 1500 CE, so the timing of maximum snowline lowering must postdate 1500 CE. Having demonstrated that clusters of kill dates align with centuries of simulated cold summers in the past2k simulation and that past2k temperature trends align with the Dewar Lakes summer temperature record of the past 50 years, we rely on the past2k simulation to estimate the timing of peak snowline lowering defined by sparsely vegetated regions in remote imagery. In the past2k simulation from 1500 to 2000 CE (Fig. 14), the irregular decline in summer temperature reaches its lowest values between 1780 and 1880 CE, the coldest century of the Common Era. Subsequently, temperatures rose steadily to the warm decades of the 1930s–1950s CE. We conclude that the ice caps that killed vegetation apparent in remote imagery persisted for at least the 100 years of cold summers between 1780 and 1880 CE.

5.2   Comparing Baffin Island kill date records with a continuous proxy record of ice cap expansion in Iceland though the Common Era

The composite PDF of 186 kill dates from 70 ice caps (Fig. 10c) provides a direct record of past ice cap expansion, with changes in mean summer temperature as the primary control on ice cap dimensions. A major advantage of
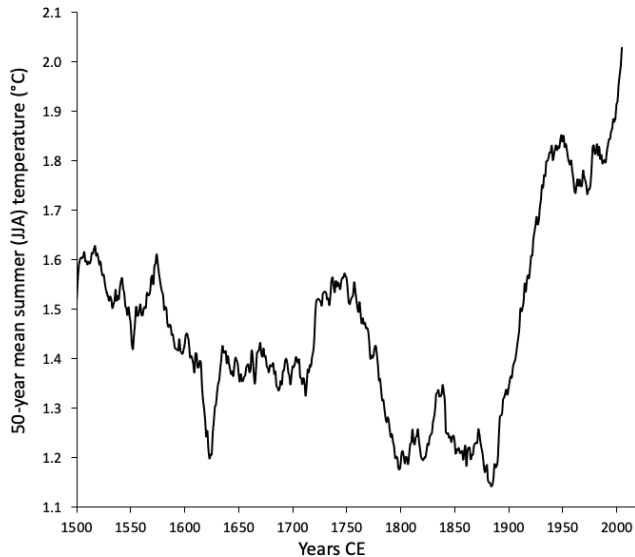
Figure 14. The 50-year running means of summer (JJA) temperatures in our past2k simulation illustrating the strong trend in declining summer temperatures after 1500 CE (our youngest kill dates), the peak cold century (1780–1880 CE) and rapid summer temperature rise after 1900 CE.

our data set is that moss kill dates require no training sets for their interpretation. Although they are discontinuous records, the discontinuities are important. Consequently, they differ in significant ways from continuous records of glacier dimen-
5 sion proxies. To evaluate whether the Baffin kill date record reflects the evolution of summer temperature for the North Atlantic Arctic, as suggested by the strong correlation with climate model results for those lands, we compare the discontinuous moss kill date record that defines time of glacier
10 expansion on Baffin Island with a continuous, annually resolved Common Era record of glacier dimensions from Iceland, also a part of the North Atlantic Arctic lands included in our model.

The Iceland record is derived from annual varve thick-
15 nesses in a sediment core from glacial lake Hvítárvatn that drains Langjökull, the second-largest ice cap in Iceland. Two primary Langjökull outlet glaciers drain into the lake, and during the Little Ice Age these terminated in the lake. Varve thicknesses are a direct measure of glacier dimensions; as
20 the glacier grows, more erosion occurs, and consequently, thicker annual sediment packets are recorded in Hvítárvatn. Because Hvítárvatn freezes in winter and Langjökull occupies easily eroded basaltic terrain, Hvítárvatn sediment is characterized by high sedimentation rates and consequently
25 measurable annual varve couplets for the past 3000 years or more (Larsen et al., 2011).

The Hvítárvatn varve thickness record over the Common Era is plotted against the moss kill date record in Fig. 15. Varve thicknesses are low but easily measured at the start of
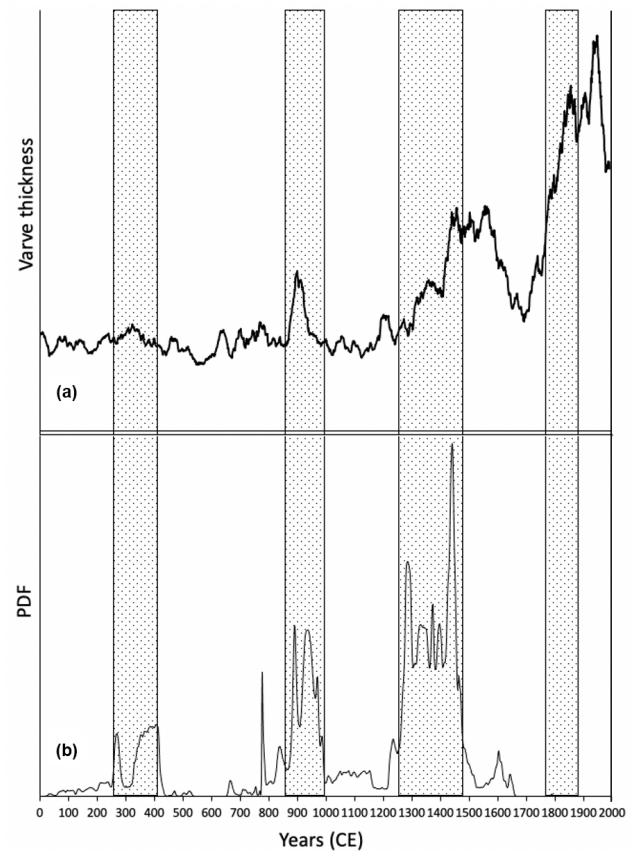30 the Common Era. There is a slight increase in varve thick-

Figure 15. Comparison of 15-year running means of annual varve thickness in the glacial lake Hvítárvatn (**a**), a proxy for the size of Langjökull, the second-largest glacier in Iceland, and 186 moss kill dates from Baffin Island (**b**). Stippled boxes show the close correspondence between the growth of Langjökull and the expansion of Baffin Island ice caps. The varves also confirm that Langjökull attained its greatest dimensions in the late 1800s CE, the same time the Baffin Island snowline was at its lowest in the Common Era. The close correspondence of the two paleoclimate records suggest Baffin kill dates and Hvítárvatn varves provide a broader North Atlantic Arctic temperature history for the Common Era.

ness at 250–450 CE, coincident with the first cluster of kill dates. A more prominent spike in varve thickness that occurs between 850 and 950 CE is coincident with the second Baffin Island kill date clusters between 850 and 1000 CE. The final kill date cluster (1240–1480 CE) is represented in the 35 Hvítárvatn varve record by increasing varve thicknesses that double between 1240 and 1480 CE. Our estimated age for the lowest Baffin Island snowline (1780–1880 CE) is matched by Langjökull varves remaining relatively thick after 1480 CE until thickening rapidly between 1780 and 1880 CE, when 40 the outlet glaciers terminated in the lake (Larsen et al., 2011). Although historical records confirm Langjökull has been receding since ∼ 1900 CE, Hvítárvatn varves remain thick because Langjökull is much thicker (∼ 600 m) than Baffin Is-

land upland ice caps, and it thus has a longer time constant when responding to large increases in summer temperature.

The commonalities between the Hvítárvatn varve thicknesses record as a proxy for Langjökull dimensions and moss kill dates representing episodes of Baffin Island ice cap expansion suggests both data sets provide a similar record of regional North Atlantic Arctic summer climate through the Common Era. Most other Arctic Common Era summer temperature reconstructions are pan-Arctic (e.g., McKay and Kaufman, 2014 TS15; Werner et al., 2018) and show summer temperature variability through the first millennium CE but without a trend, which differs from our records that show overall summer cooling through the same time interval. The difference is likely because those records are pan-Arctic, whereas our results are limited to the North Atlantic Arctic where the sea ice feedback is stronger, and climate modeling shows pan-Arctic spatial gradients in response to natural forcing over the Common Era (Zhong et al., 2018).

5.3   Evolution of the Baffin Island snowline through the Common Era

The PDF of all moss kill dates (Fig. 10c) defines three episodes of Common Era ice cap expansion. We derive an estimate of the corresponding snowline during each expansion from the mean elevation of the lowest 20 % of all dated sites for each interval. We define snowline as the lowest elevation that snow or ice persisted long enough to kill all vegetation (multiple decades), sufficient time for snow to turn into ice. During times of lowering snowline, ice margins expand at many elevations. But because the ice caps are cold based and ice velocities are negligible, the lowest ice margins are the closest quantitative estimate of snowline available. We recognize that ice cap margins defined by their kill dates may be smaller than their maximum dimensions due to ice recession before reburial under a younger ice cap, but those elevations remain the best estimate for the minimum snowline lowering. We estimate snowline at the peak Little Ice Age from the lowest persistent elevation of remnant vegetation trimlines (Fig. 2) and assign an age of 1880 CE to that snowline, as discussed in Sect. 5.1.

During the Common Era, the snowline declined more than 400 m, from an initial elevation above 900 m a.s.l. to the sparsely vegetated hills 450 to 500 m a.s.l. To evaluate how a declining snowline elevation translates to the area of permanent ice, we calculate the distribution of area across elevations for the region of low-vegetation cover outlined in Fig. 1. Reconstructed snowline elevations for the three kill date clusters are mapped on to the area–elevation relationship (Fig. S3). To calculate the area of permanent ice cover at peak LIA cold, we measured the area of sparsely vegetated regions (Fig. S4). Figure 16 illustrates the highly nonlinear relationship between snowline decline and resultant areal extent of permanent ice. Although we lack quantitative snowline data between ice cap advances, the snowline could not
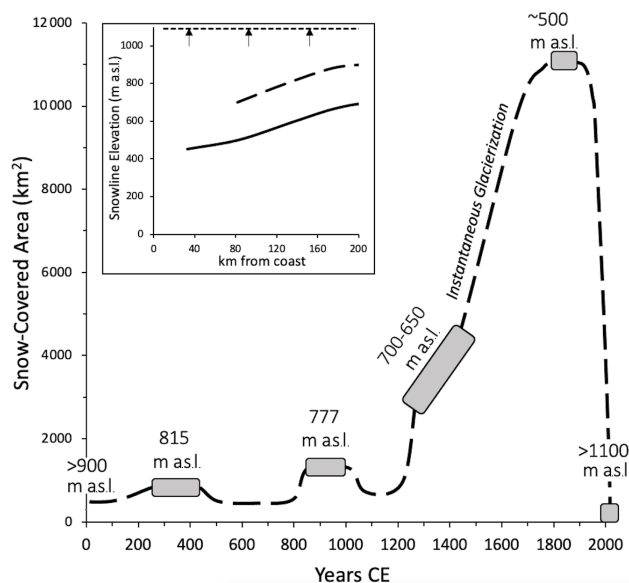

Figure 16. Changes in ice-covered area through the Common Era within our prescribed field area (Fig. 1). Episodes of ice cap expansion derived from moss kill dates (Fig. 10c; square boxes), with their associated snowline elevation listed above each box, are plotted against the ice-covered area based on the area–elevation relation within the field area as shown in Fig. S3. The area covered by ice caps for 1780–1880 CE is the summed area defined by vegetation trim lines (Fig. S4), with the age derived from the past2k modeled temperatures (Sect. 5.1). The inset shows the snowline elevations throughout our field area for 1880 CE (solid line) and 1960 CE (dashed line), whereas the snowline is currently above 2020 CE everywhere (dotted line) CE5. The dramatic increase in area of permanently covered ice as snowline descended through the Little Ice Age was originally postulated by Ives (1957) to result in "instantaneous glacierization" due to the significant albedo increase that might lead to the onset of an ice age (Andrews and Mahaffy, 1975; Clark et al., 1993; Birch et al., 2017).

have risen much above the preceding low snowline for long because all ice from earlier advances would have melted and no dead vegetation would have been preserved.

5.4   "Instantaneous glacierization" and the initiation of the Laurentide Ice Sheet

The large area of the north-central Baffin Island uplands ice covered at the peak of the Little Ice Age relative to the area currently glacierized (e.g., Fig. 2) led to the concept of "instantaneous glacierization" (Ives, 1957; Andrews et al., 1975; Ives et al., 1975) when a modest decline in snowline can result in a dramatic increase in the area beneath ice caps. Subsequent simulations of conditions leading to the initiation of the Laurentide Ice Sheet from an initial interglacial state (e.g., Andrews and Mahaffy, 1975 TS16; Clark et al., 1993; Kleman et al., 2002; Birch et al., 2017, 2018) all show initial

snow accumulation on Baffin Island, with the albedo feedback providing an important acceleration of ice sheet growth.

The dramatic increase in the area under permanent snow or ice cover in our field area between 1480 and 1880 CE (Fig. 15), during which time the snowline dropped 165 m from ∼ 665 to ∼ 500 m a.s.l., is due to the large area of land between those two elevations (Fig. S3). Assuming a standard free-air lapse rate of 0.6 °C per 100 m, this drop in snowline required only a 1 °C decrease in mean summer temperature. The direct evidence of "instantaneous glacierization", constrained by the limits provided by moss kill dates and climate modeling illustrates how a significant albedo increase may occur following a modest decrease in summer temperature, where the resultant snowline descent results in a dramatic increase in permanently ice-covered lands.

5.5 Climate forcing that led to 20th-century ice cap recession

The combination of direct evidence and modeled summer temperatures points to rapid recession from maximum Common Era ice cap coverage across north-central Baffin Island beginning in the late 1800s CE. The past2k model simulates all summers after 1900 CE warmer than the mean summer temperature of the 19th century, with particularly warm summers seen between 1920 and 1960 CE (Figs. 14 and 16), similar to Arctic-wide temperatures in multiple climate model simulations with all forcings (Fyfe et al., 2013). The dominant forcings that contribute to warming from 1900 to 1960, by which time remote imagery shows that almost all peak LIA ice caps in the field area (Fig. 2) had melted, include a slight increase in solar irradiance through the early 1900s, significant increases in greenhouse gases (GHGs: CO_2, CH_4, and N_2O; Fig. 4) that are partially compensated by a cooling effect from increased anthropogenic aerosols and land use change, and a very slight decline in Northern Hemisphere summer insolation from orbital terms (e.g., Fyfe et al., 2013).

An underlying question is whether the cold century from 1780 to 1880 CE and resultant dramatic increase in ice-covered terrain across north-central Baffin Island was the prelude to a transition into a new ice age or just an aberrant century that even without anthropogenic trace gas inputs would have returned to warmer summers and ice cap retreat. The primary impacts on Earth's planetary energy balance over the past century are the opposing effects of anthropogenic aerosols and greenhouse gases, with modest impacts from solar irradiance and volcanism (Myhre et al., 2013; Zhao et al., 2019).

Fyfe et al. (2013) compared pan-Arctic mean annual temperature anomalies over the 20th century in a range of models that included those using only natural forcings (solar irradiance and volcanism) and those using historical forcings (natural forcings plus greenhouse gas and aerosol forcings). They found that natural simulations resulted in no trend in circum-Arctic mean annual temperatures, whereas historical
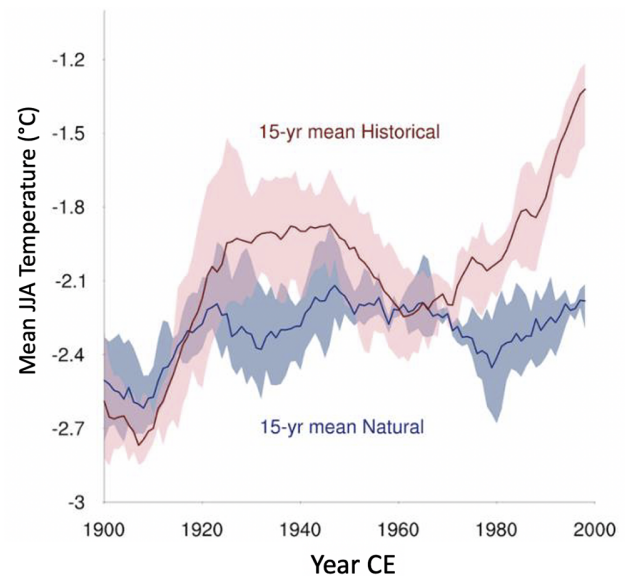

Figure 17. Comparison of 15-year running means of summer (JJA) temperatures over Arctic land area north of 60° N and between 30° E and 90° W for CESM-1 simulations initiated in 1850 CE with historical forcings (natural + anthropogenic; four runs) and only natural forcings (TSI, volcanism, insolation; three runs) for the 20th century. Red and blue curves are ensemble means of the four historical runs and the three natural runs, respectively, with the ±1σ TS17 ranges of the ensemble runs given by the shading. The early 20th-century rise in the historical simulation is due primarily to GHG increases, with the subsequent decline primarily a result of additions of aerosols, which are reduced somewhat after 1960 as the continued increase in GHG dominates change. In contrast, there is no significant trend in the natural simulations after 1920 CE.

simulations produced a modest early 20th-century temperature rise, a slight decline in temperature centered on the 1960s, and a steady warming thereafter. However, the Fyfe et al. (2013) results cannot be compared in detail to our reconstructed changes in the North Atlantic sector, which behave differently from the pan-Arctic average in paleoclimate models (Zhong et al., 2018). Their conclusions also were for mean annual temperatures, whereas we focus on mean summer temperature, the primary control on glacier mass balance (Koerner, 2005).

To test the potential role of anthropogenic forcing in the observed Baffin Island snowline rise after 1880 CE we compare 15-year running means of summer (JJA) temperature over the North Atlantic Arctic lands in a series of CESM1 ensembles beginning in 1850 CE with historical (four runs) and CESM1 ensembles with only natural forcings (three runs; Hurrell et al., 2013; Meehl et al., 2020; Xu et al., 2022) in Fig. 17. The historical and natural ensembles track closely until ∼ 1920 CE, when the historical ensemble continues a long increase in simulated summer temperature, with a temporary reduction in the 1950s and 1960s, whereas the natural forcing simulations fail to show additional increases in

summer temperature after 1920. Based on this comparison, it is likely that some rise in snowline in the early 1990s would have occurred without any anthropogenic disturbance in the planetary energy balance, but the significant increase in summer temperatures after 1920 CE seen in both the past2k and historical simulations is primarily a response to anthropogenic impacts. This suggests that without anthropogenic impacts Baffin Island ice caps would still be widespread at elevations well below 600 m a.s.l., the lowest elevation ice cap in 1985 CE imagery (Fig. 2).

6   Conclusions

– Most ice caps mantling the cold, low-relief landscapes of Baffin Island are frozen to their beds, allowing them to act as preservation agents. Ice cap dimensions are set by summer temperature, with small changes in summer temperature driving significant changes in glacier dimensions. As ice caps expand, they entomb vegetation in situ, preserving them until the vegetation is re-exposed when ice caps recede. Radiocarbon dates on moss collected within a few meters of ice cap margins date times of consistently cold summers resulting in ice cap expansion through the Common Era but are restricted to expansions for which subsequent summers never warmed sufficiently and/or long enough to completely melt earlier ice cap expansions. By inference, summers currently are warmer than any series of multidecadal summers since the dated ice cap expansions, placing contemporary warming in a millennial perspective. Kill dates that define changes in ice cap dimensions provide a reliable summer paleotemperature proxy.

– None of the 107 kill dates from plateau ice caps within the area inscribed in Fig. 1 pre-date the Common Era. Consequently, if earlier Neoglacial episodes of summer cold resulted in long-lived ice caps across the uplands, subsequent summers were warm enough and/or long enough to completely melt those ice caps before 1 CE.

– The composite PDF of 186 moss Common Era kill dates collected from 70 ice caps over a region covering more than 50 000 km^2 yields three multi-century clusters, defining times of widespread ice cap expansion at 250–450 CE, 850–1000 CE, and 1240–1480 CE; ice margins continued to expand after 1480 CE to a peak snowline lowering between 1780 and 1880 CE, resulting in over $\sim 11\,000$ km^2 covered by ice caps, across a region where ice caps currently cover < 100 km^2.

– Intervals of ice cap expansion defined by moss kill dates through the Common Era align with centuries of persistent cold summers in the past2k fully coupled climate model for the Common Era with all major forcings. The model simulates decadally averaged summer temperatures that reveal a first-order decline in summer temperatures over the Common Era, consistent with peak Neoglacial ice dimensions late in the Little Ice Age. Centennial intervals of cold summers align with the clusters of kill dates; warm modeled summers align with intervals lacking kill dates. Peak Common Era modeled cold summers between 1780 and 1880 CE led to a snowline decline that dramatically increased the snow-covered regions of the Baffin Island uplands (instantaneous glacierization) and brought the eastern Canadian Arctic perilously close to conditions anticipated at the inception phase of the Laurentide Ice Sheet.

– Climate modeling over the interval from 1850 CE to present suggests that rapid ice cap retreat over Baffin Island beginning ~ 1880 CE, but especially after 1920 CE, was driven primarily by anthropogenic forcing. We may never know with certainty whether the dramatic snowline decline and resultant aerial increase in permanently snow-covered lands in Arctic Canada at the peak of the Little Ice Age heralded the onset of the next Northern Hemisphere ice age, only to be reversed by the increase in greenhouse gases and other forcing agents related to the Industrial Revolution. Summer insolation across the Arctic was near its orbitally driven minimum at the peak of the Little Ice Age and will continue to decrease slightly through the 21st century. The strong positive correlation between Arctic summer temperatures and summer insolation (Kaufman et al., 2009 TS18) suggests that only the additional anthropogenic forcings since ~ 1850 CE reversed the natural transition into a new ice age.

– Clusters of kill dates that define multidecadal episodes of expanding Baffin Island Ice Caps align with expanding margins of Langjökull, the second-largest ice cap in Iceland, as recorded in an annually resolved continuous record through the Common Era from the glacial lake Hvítárvatn. This correlation suggests our record provides a North Atlantic Arctic template for Common Era summer temperatures, with the coldest century of the Common Era occurring between 1780 and 1880 CE.

The 186 moss kill dates, including their location and calibration, are available at https://doi.org/10.18739/A2RN30884 (Pendleton and Miller, 2023).

References

.TS24

Anderson, R. K., Miller, G. H., Briner, J. P., Lifton, N. A., and DeVogel, S. B.: A millennial perspective on Arctic warming from ^{14}C in quartz and plants emerging from beneath ice caps. 2008, Geophys. Res. Lett., 35, L01502, https://doi.org/10.1029/2007GL032057, 2008.

Andrews, J. T. and Mahaffy, M. A. W.: Growth Rate of the Laurentide Ice Sheet and Sea Level Lowering (with Emphasis on the 115,000 BP Sea Level Low), Quaternary Res., 6, 167–83, 1976. TS25

Andrews, J. T., Davis, P. T., Wright, C.: Little Ice Age permanent snowcover in the Eastern Canadian Arctic: Extent mapper from LandSat-1 satellite imagery, Geog. Annaler, 58A, 71–81, 1976.

Birch, L., Cronin, T., and Tziperman, E.: Glacial Inception on Baffin Island: The Role of Insolation, Meteorology, and Topography, J. Climate, 30, 4047–4064, https://doi.org/10.1175/JCLI-D-16-0576.1, 2017.

Birch, L., Cronin, T., and Tziperman, E.: The role of regional feedbacks in glacial inception on Baffin Island: the interaction of ice flow and meteorology, Clim. Past, 14, 1441–1462, https://doi.org/10.5194/cp-14-1441-2018, 2018.

Briner, J. P., Michelutti, N., Francis, D. R., Miller, G. H., Axford, Y., Wooller, M. J., Wolfe, A. P., Axford, Y., and Wolfe, A. P.: A Multi-Proxy Lacustrine Record of Holocene Climate Change on Northeastern Baffin Island, Arctic Canada, Quaternary Res., 65, 431–442, https://doi.org/10.1016/j.yqres.2005.10.005, 2006.

Briner, J. P., Davis, P. T., and Miller, G. H.: Latest Pleistocene and Holocene Glaciation of Baffin Island, Arctic Canada: Key Patterns and Chronologies, Quaternary Sci. Rev., 28, 2075–2087, 2009.

Briner, J. P., McKay, N. P., Axford, Y., Bennike, O., Bradley, R. S., de Vernal, A., Fisher, D., TS26 et al.: Holocene Climate Change in Arctic Canada and Greenland, Quaternary Sci. Rev., 147, 340–364, https://doi.org/10.1016/j.quascirev.2016.02.010, 2016.

Büntgen, U., Myglan, V. S., Charpentier Ljungqvist, F., McCormick, M., Di Cosmo, N., Sigl, M., Jungclaus, J., TS27 et al.: Cooling and Societal Change during the Late Antique Little Ice Age from 536 to around 660 AD, Nat. Geosci., 9, 231–236, https://doi.org/10.1038/ngeo2652, 2016.

Calkin, P. E. and Ellis, J. M.: A Cirque-Glacier Chronology Based on Emergent Lichens and Mosses, J. Glaciol., 27, 511–515, https://doi.org/10.1017/S0022143000011576, 1981.

Clark, P. U.: Unstable Behavior of the Laurentide Ice Sheet over Deforming Sediment and Its Implications for Climate Change, Quaternary Res., TS28 https://doi.org/10.1006/qres.1994.1002, 1994. TS29

Clark, P. U., Clague, J. J., Curry, B. B., Dreimanis, A., Hicock, S. R., Miller, G. H., Berger, G. W., TS30 et al.: Initiation and Development of the Laurentide and Cordilleran Ice Sheets Following the Last Interglaciation, Quaternary Sci. Rev., 12, 79–114, https://doi.org/10.1016/0277-3791(93)90011-A, 1993.

Climate Data Gateway at NCAR: Past2k: Transient simulation of the climate of the last 2000 years, NCAR [data

set], https://www.earthsystemgrid.org/dataset/ucar.cgd.ccsm4.past2k_transient.html (last access: TS31), 2021.TS32

Crump, S. E., Anderson, L. S., Miller, G. H., and Anderson, R. S.: Interpreting Exposure Ages from Ice-Cored Moraines: A Neoglacial Case Study on Baffin Island, Arctic Canada, J. Quaternary Sci., TS33, https://doi.org/10.1002/jqs.2979, 2017.

Deser, C., Phillips, A. S., Simpson, I. R., Rosenbloom, N., Coleman, D., Lehner, F., Pendergrass, A. G., Dinezio, P., and Stevenson, S.: Isolating the Evolving Contributions of Anthropogenic Aerosols and Greenhouse Gases: A New CESM1 Large Ensemble Community Resource, J. Climate, 33, 7835–7858, https://doi.org/10.1175/JCLI-D-20-0123.1, 2020.TS34

Dyke, A. S.: An Outline of North American Deglaciation with Emphasis on Central and Northern Canada, Developments in Quaternary Science, 2, 373–424, https://doi.org/10.1016/S1571-0866(04)80209-4, 2004.

Francis, J. A., Vavrus, S. J., and Cohen, J.: Amplified Arctic Warming and Mid-Latitude Weather: New Perspectives on Emerging Connections, Wiley Interdisciplinary Reviews: Climate Change, 8, 1–11, https://doi.org/10.1002/wcc.474, 2017.TS35

Fyfe, J. C., Von Salzen, K., Gillett, N. P., Arora, V. K., Flato, G. M., and McConnell, J. R.: One Hundred Years of Arctic Surface Temperature Variation Due to Anthropogenic Influence, Sci. Rep.-UKTS36, 3, 1–7, https://doi.org/10.1038/srep02645, 2013.

Gardner, A., Moholdt, G., Arendt, A., and Wouters, B.: Accelerated contributions of Canada's Baffin and Bylot Island glaciers to sea level rise over the past half century, The Cryosphere, 6, 1103–1125, https://doi.org/10.5194/tc-6-1103-2012, 2012.

Goldewijk, K., Beusen, A., Van Drecht, G., and De Vos, M.: The HYDE 3.1 spatially explicit database of human-induced global land-use change over the past 12,000 years, Global Ecol. Biogeogr., 20, 73–86, https://doi.org/10.1111/j.1466-8238.2010.00587.x, 2011.

Groff, D. V., Beilman, D. W., Yu, Z., Ford, D., and Xia, Z.: Kill Dates from Re-Exposed Black Mosses Constrain Past Glacier Advances in the Northern Antarctic Peninsula, Geology, 51, 257–261, https://doi.org/10.1130/g50314.1, 2023.

Harning, D. J., Geirsdóttir, Á., Miller, G. H., and Anderson, L.: Episodic Expansion of Drangajökull, Vestfirðir, Iceland, over the Last 3 Ka Culminating in Its Maximum Dimension during the Little Ice Age, Quaternary Sci. Rev., 152, 118–131, https://doi.org/10.1016/j.quascirev.2016.10.001, 2016.

Hugonnet, R., McNabb, R., Berthier, E., TS37, et al.: Accelerated global glacier mass loss in the early twenty-first century, Nature, 592, 726–731, https://doi.org/10.1038/s41586-021-03436-z, 2021.TS38

Hurrell, J. W., Holland, M. M., Gent, P. R., Ghan, S., Kay, J. E., Kushner, P. J., Lamarque, J. F., TS39, et al.: The Community Earth System Model: A Framework for Collaborative Research, B. Am. Meteorol. Soc., 94, 1339–1360, https://doi.org/10.1175/BAMS-D-12-00121.1, 2013.

Ives, J. D.: Glaciation of the Torngat Mountains, Northern Labrador, Arctic, 10, 67–87, 1957.

Ives, J. D.: Indications of recent extensive glacierization in north-central Baffin Island, NWT, J. Glaciol., 4, 197–205, https://doi.org/10.3189/S0022143000027398, 1962.

Ives, J. D., Andrews, J. T., and Barry, R. G.: Growth and Decay of the Laurentide Ice Sheet and Comparisons with Fenno-Scandinavia, Die Naturwissenschaften, 62, 118–125, 1975.

Jungclaus, J. H., Bard, E., Baroni, M., Braconnot, P., Cao, J., Chini, L. P., Egorova, T., Evans, M., González-Rouco, J. F., Goosse, H., Hurtt, G. C., Joos, F., Kaplan, J. O., Khodri, M., Klein Goldewijk, K., Krivova, N., LeGrande, A. N., Lorenz, S. J., Luterbacher, J., Man, W., Maycock, A. C., Meinshausen, M., Moberg, A., Muscheler, R., Nehrbass-Ahles, C., Otto-Bliesner, B. I., Phipps, S. J., Pongratz, J., Rozanov, E., Schmidt, G. A., Schmidt, H., Schmutz, W., Schurer, A., Shapiro, A. I., Sigl, M., Smerdon, J. E., Solanki, S. K., Timmreck, C., Toohey, M., Usoskin, I. G., Wagner, S., Wu, C.-J., Yeo, K. L., Zanchettin, D., Zhang, Q., and Zorita, E.: The PMIP4 contribution to CMIP6 – Part 3: The last millennium, scientific objective, and experimental design for the PMIP4 past1000 simulations, Geosci. Model Dev., 10, 4005–4033, https://doi.org/10.5194/gmd-10-4005-2017, 2017.

Kleman, J., Fastook, J., and Stroeven, A. P.: Geologically and Geomorphologically Constrained Numerical Model of Laurentide Ice Sheet Inception and Build-Up, Quaternary Int., 95–96, 87–98, 2002.

Koerner, R. M.: Mass Balance of Glaciers in the Queen Elizabeth Islands, Nunavut, Canada, Ann. Glaciol., 42, 417–423, https://doi.org/10.3189/172756405781813122, 2005.

Larsen, D. J., Miller, G. H., Geirsdóttir, Á., and Thordarson, T.: A 3000-Year Varved Record of Glacier Activity and Climate Change from the Proglacial Lake Hvítárvatn, Iceland, Quaternary Sci. Rev., 30, 19–20, https://doi.org/10.1016/j.quascirev.2011.05.026, 2011.

Lecavalier, B. S., Fisher, D. A., Milne, G. A., Vinther, B. M., Tarasov, L., Huybrechts, P., Lacelle, D., TS40, et al.: High Arctic Holocene Temperature Record from the Agassiz Ice Cap and Greenland Ice Sheet Evolution, P. Natl. Acad. Sci. USA, 114, 5952–5957, https://doi.org/10.1073/pnas.1616287114, 2017.

Lenaerts, J. T. M., Van Angelen, J. H., Van Den Broeke, M. R., Gardner, A. S., Wouters, B., and Van Meijgaard, E.: Irreversible Mass Loss of Canadian Arctic Archipelago Glaciers, Geophys. Res. Lett., 40, 870–874, https://doi.org/10.1002/grl.50214, 2013.

Locke, C. W. and Locke III, W. L.: Little Ice Age Snow-Cover Extent and Paleoglaciation Thresholds: North-Central Baffin Island, N.W.T., Canada, Arct. Alp. Res., 23, 436–443, 1991.TS41

Lowell, T. V., Hall, B. L., Kelly, M. A., Bennike, O., Lusas, A. R., Honsaker, W., Smith, C. A., Levy, L. B., Travis, S., and Denton, G. H.: Late Holocene Expansion of Istorvet Ice Cap, Liverpool Land, East Greenland, Quaternary Sci. Rev., 63, 128–140, https://doi.org/10.1016/j.quascirev.2012.11.012, 2013.

z MacFarling Meure, C., Etheridge, D., Trudinger, C., Steele, P., Langenfelds, R., Van Ommen, T., Smith, A., and Elkins, J.: Law Dome CO_2, CH_4 and N_2O Ice Core Records Extended to 2000 Years BP, Geophys. Res. Lett., 33, 2000–2003, https://doi.org/10.1029/2006GL026152, 2006.

Margreth, A., Dyke, A. S., Gosse, J. C., and Telka, A. M.: Neoglacial Ice Expansion and Late Holocene Cold-Based Ice Cap Dynamics on Cumberland Peninsula, Baffin Island, Arctic Canada, Quaternary Sci. Rev., 91, 242–256, https://doi.org/10.1016/j.quascirev.2014.02.005, 2014.

Medford, A. K., Hall, B. L., Lowell, T. V., Kelly, M. A., Levy, L. B., Wilcox, P. S., and Axford, Y.: Holocene Glacial History of Renland Ice Cap, East Greenland, Reconstructed from Lake Sediments, Quaternary Sci. Rev., 258, 106883, https://doi.org/10.1016/j.quascirev.2021.106883, 2021.

Medrzycka, D., Copland, L., and Noël, B.: Rapid Demise and Committed Loss of Bowman Glacier, Northern Ellesmere Island, Arctic Canada, J. Glaciol., TS42, 1–14, https://doi.org/10.1017/jog.2022.119, 2023. TS43

Meehl, G. A., Hu, A., Castruccio, F., England, M. H., Bates, S. C., Donabasoglu, G., McGregor, S., Arblaster, J. M., Xie, S.-P., and Rosenbloom, N.: Atlantic and Pacific tropics connected by mutually interactive decadal-timescale processes, Nat. Geosci., TS44, https://doi.org/10.1038/s41561-020-00669-x, 2020.

Miller, G. H.: Late Quaternary Glacial and Climatic History of Northern Cumberland Peninsula, Baffin Island, N.W.T., Canada, Quaternary Res., 3, 561–583, 1973.

Miller, G. H., Wolfe, A. P., Briner, J. P., Sauer, P. E., and Nesje, A.: Holocene Glaciation and Climate Evolution of Baffin Island, Arctic Canada, Quaternary Sci. Rev., 24, 1703–1721, https://doi.org/10.1016/j.quascirev.2004.06.021, 2005.

Miller, G. H., Alley, R. B., Brigham-Grette, J., Fitzpatrick, J. J., Polyak, L., Serreze, M. C., and White, J. W. C.: Arctic Amplification: Can the Past Constrain the Future?, Quaternary Sci. Rev., 29, 1779–1790, https://doi.org/10.1016/j.quascirev.2010.02.008, 2010.

Miller, G. H., Geirsdottir, A., Zhong, Y., Larsen, D. J., Otto-Bliesner, B., Holland, M. M., Bailey, D. A., TS45, et al.: Abrupt Onset of the Little Ice Age Triggered by Volcanism and Sustained by Sea-Ice/Ocean Feedbacks, Geophys. Res. Lett., 39, TS46, https://doi.org/10.1029/2011GL050168, 2012.

Miller, G. H., Lehman, S. J., Refsnider, K. A., Southon, J. R., and Zhong, Y.: Unprecedented Recent Summer Warmth in Arctic Canada, Geophys. Res. Lett., 40, 5745–5751, https://doi.org/10.1002/2013GL057188, 2013.

Miller, G. H., Landvik, J. Y., Lehman, S. J., and Southon, J. R.: Episodic Neoglacial Snowline Descent and Glacier Expansion on Svalbard Reconstructed from the ^{14}C Ages of Ice-Entombed Plants, Quaternary Sci. Rev., 155, TS47, https://doi.org/10.1016/j.quascirev.2016.10.023, 2017.

Moore, J. J., Kughen, K. A., Miller, G. H., and Overpeck, J. T.: Little Ice Age Recorded in Summer Temperature Reconstruction from Varved Sediments of Donard Lake, Baffin Island, Canada, J. Paleolimnol., 25, 503–517, https://doi.org/10.1023/A:1011181301514, 2001.

Myhre, G., Samset, B. H., Schulz, M., Balkanski, Y., Bauer, S., Berntsen, T. K., Bian, H., Bellouin, N., Chin, M., Diehl, T., Easter, R. C., Feichter, J., Ghan, S. J., Hauglustaine, D., Iversen, T., Kinne, S., Kirkevåg, A., Lamarque, J.-F., Lin, G., Liu, X., Lund, M. T., Luo, G., Ma, X., van Noije, T., Penner, J. E., Rasch, P. J., Ruiz, A., Seland, Ø., Skeie, R. B., Stier, P., Takemura, T., Tsigaridis, K., Wang, P., Wang, Z., Xu, L., Yu, H., Yu, F., Yoon, J.-H., Zhang, K., Zhang, H., and Zhou, C.: Radiative forcing of the direct aerosol effect from AeroCom Phase II simulations, Atmos. Chem. Phys., 13, 1853–1877, https://doi.org/10.5194/acp-13-1853-2013, 2013.

Noël, B., van de Berg, W. J., Lhermitte, S., Wouters, B., Schaffer, N., and van den Broeke, M. R.: Six Decades of Glacial Mass Loss in the Canadian Arctic Archipelago, J. Geophys. Res.-Earth Surf., 123, 1430–1449, https://doi.org/10.1029/2017JF004304, 2018.

Otto-Bliesner, B. L., Brady, E. C., Fasullo, J., Jahn, A., Landrum, L., Stevenson, S., Rosenbloom, N., Mai, A., and Strand, G.: Climate Variability and Change since 850 Ce an Ensemble Approach with the Community Earth System Model, B. Am. Meteorol. Soc., 97, 787–801, https://doi.org/10.1175/BAMS-D-14-00233.1, 2016.

Pendleton, S. and Miller, G.: Radiocarbon dates and their probability density distributions for moss samples killed by expanding ice caps on northern Baffin Island, NU, Canada, 2005–2019, Arctic Data Center [data set], https://doi.org/10.18739/A2RN30884, 2023. TS48

Pendleton, S. L., Miller, G. H., Anderson, R. A., Crump, S. E., Zhong, Y., Jahn, A., and Geirsdottir, Á.: Episodic Neoglacial expansion and rapid 20th century retreat of a small ice cap on Baffin Island, Arctic Canada, and modeled temperature change, Clim. Past, 13, 1527–1537, https://doi.org/10.5194/cp-13-1527-2017, 2017.

Pendleton, S. L., Miller, G. H., Lifton, N., Lehman, S. J., Southon, J., Crump, S. E., and Anderson, R. S.: Rapidly Receding Arctic Canada Glaciers Revealing Landscapes Continuously Ice-Covered for More than 40,000 Years, Nat. Commun., 10, 1–8, https://doi.org/10.1038/s41467-019-08307-w, 2019a.

Pendleton, S., Miller, G., Lifton, N., and Young, N.: Cryosphere Response Resolves Conflicting Evidence for the Timing of Peak Holocene Warmth on Baffin Island, Arctic Canada, Quaternary Sci. Rev., 216, 107–115, https://doi.org/10.1016/j.quascirev.2019.05.015, 2019b.

Ramsey, C. B., Staff, R. A., Bryant, C. L., Brock, F., Kitagawa, H., Van Der Plicht, J., Schlolaut, G., TS49, et al.: A Complete Terrestrial Radiocarbon Record for 11.2 to 52.8 Kyr B.P., Science, 338, 370–374, https://doi.org/10.1126/science.1226660, 2012. TS50

Rantanen, M., Karpechko, A. Y., Lipponen, A., Nordling, K., Hyvärinen, O., Ruosteenoja, K., Vihma, T., and Laaksonen, A.: The Arctic has warmed nearly four times faster than the globe since 1979, Commun. Earth Environ., 3, 168 TS51, 2022.

Reimer, P. J., Austin, W. E. N., Bard, E., Bayliss, A., Blackwell, P. G., Ramsey, C. B., Butzin, M., TS52, et al.: The IntCal20 Northern Hemisphere Radiocarbon Age Calibration Curve (0–55 Cal KBP), Radiocarbon, 62, 725–757, https://doi.org/10.1017/RDC.2020.41, 2020.

Schweinsberg, A. D., Briner, J. P., Miller, G. H., Bennike, O., and Thomas, E. K.: Local Glaciation in West Greenland Linked to North Atlantic Ocean Circulation during the Holocene, Geology, 45, TS53, https://doi.org/10.1130/G38114.1, 2017.

Schweinsberg, A. D., Briner, J. P., Miller, G. H., Lifton, N. A., Bennike, O., and Graham, B. L.: Holocene Mountain Glacier History in the Sukkertoppen Iskappe Area, Southwest Greenland, Quaternary Sci. Rev., 197, 142–161, https://doi.org/10.1016/j.quascirev.2018.06.014, 2018.

Serreze, M. C., Barrett, A. P., Stroeve, J. C., Kindig, D. N., and Holland, M. M.: The emergence of surface-based Arctic amplification, The Cryosphere, 3, 11–19, https://doi.org/10.5194/tc-3-11-2009, 2009. TS54

Sigl, M., TS55, et al.: Timing and climate forcing of volcanic eruptions for the past 2,500 years, Nature, 523, 543–549, 2015.

Søndergaard, A. S., Krog Larsen, N., Olsen, J., Strunk, A., and Woodroffe, S.: Glacial History of the Greenland Ice Sheet and a Local Ice Cap in Qaanaaq, Northwest Greenland, J. Quaternary Sci., 34, 536–547, https://doi.org/10.1002/jqs.3139, 2019.

Taylor, K. E., Stouffer, R. J., and Meehl, G. A.: An Overview of CMIP5 and the Experiment Design, B. Am. Meteorol. Soc., 93, 485–498, https://doi.org/10.1175/BAMS-D-11-00094.1, 2012.

Tepes, P., Gourmelen, N., Nienow, P., Tsamados, M., Shepherd, A., and Weissgerber, F.: Changes in elevation and mass of Arctic glaciers and ice caps, 2010–2017, Remote Sens. Environ., 261, 112481, https://doi.org/10.1016/j.rse.2021.112481, 2021. TS56

Werner, J. P., Divine, D. V., Charpentier Ljungqvist, F., Nilsen, T., and Francus, P.: Spatio-temporal variability of Arctic summer temperatures over the past 2 millennia, Clim. Past, 14, 527–557, https://doi.org/10.5194/cp-14-527-2018, 2018.

Williams, L. D.: The Little Ice Age Glaciation Level on Baffin Island, Arctic Canada, Palaeogeogr. Palaeocl., 25, 199–207, https://doi.org/10.1016/0031-0182(78)90036-6, 1978.

Wolken, G. J., England, J. H., and Dyke, A. S.: Re-Evaluating the Relevance of Vegetation Trimlines in the Canadian Arctic as an Indicator of Little Ice Age Paleoenvironments, Arctic, 58, 341–353, https://doi.org/10.14430/arctic448, 2005.

Xu, Y., Lin, L., Diao, C., Wang, Z., Bates, S., and Arblaster, J.: The response of precipitation extremes to the twentieth- and twenty-first-century global temperature change in a comprehensive suite of CESM1 large ensemble simulation: Revisiting the role of forcing agents vs. the role of forcing magnitudes, Earth Space Sci., 9, e2021EA002010, https://doi.org/10.1029/2021EA002010, 2022.

Zhao, A., Stevenson, D. S., and Bollasina, M. A.: Climate Forcing and Response to Greenhouse Gases, Aerosols, and Ozone in CESM1, J. Geophys. Res.-Atmos., 124, 13876–13894, https://doi.org/10.1029/2019JD030769, 2019.

Zhong, Y., Jahn, A., Miller, G. H., and Geirsdottir, A.: Asymmetric Cooling of the Atlantic and Pacific Arctic During the Past Two Millennia: A Dual Observation-Modeling Study, Geophys. Res. Lett., 45, 12497–12505, https://doi.org/10.1029/2018GL079447, 2018.

Remarks from the language copy-editor

CE1   Please provide ZIP code.
CE2   Please provide ZIP code.
CE3   Please define.
CE4   Please confirm the change.
CE5   Please confirm the change.

Remarks from the typesetter

TS1   The composition of Figs. 5–8, 10, 15 and 16 has been adjusted to our standards.
TS2   Medrzycka et al. (2022) is not in the reference list. Do you mean Medrzycka et al. (2023)?
TS3   Locke and Locke (1977) is not in the reference list.
TS4   Davis (1985) is not in the reference list.
TS5   Andrews et al. (1975) is not in the reference list.
TS6   Please provide a shorter running title.
TS7   Falconer (1966) is not in the reference list.
TS8   Please provide the corresponding citations.
TS9   Lubinski et al. (1999) is not in the reference list.
TS10   Please confirm addition of "et al.".
TS11   Yu et al. (2016) is not in the reference list.
TS12   Bronk Ramsey (2009) is not in the reference list.
TS13   Please confirm addition of citation.
TS14   Toohey et al. (2016) is not in the reference list.
TS15   McKay and Kaufman (2014) is not in the reference list.
TS16   Andrews and Mahaffy (1975) is not in the reference list. Do you mean Andrews and Mahaffy (1976)?
TS17   Please confirm change to Greek letter σ.
TS18   Kaufman et al. (2009) is not in the reference list.
TS19   Please confirm addition of citation.
TS20   Please provide a reference list entry including creators, title, and date of last access.
TS21   Please provide a reference list entry including creators, title, and date of last access.
TS22   Please provide a direct link to the data set and, if possible, a DOI instead of a URL. In any case, please provide a reference list entry including creators, title, and date of last access.
TS23   Please note that there is a discrepancy between funding information provided by you in the acknowledgements and the funding information you indicated during manuscript registration, which we used to create this section. Please double-check your acknowledgements to see whether repeated information can be removed from the acknowledgements or changed accordingly. If further funders should be added to this section, please provide the funder names and the grant numbers. Thanks.
TS24   Please ensure that any data sets and software codes used in this work are properly cited in the text and included in this reference list. Thereby, please keep our reference style in mind, including creators, titles, publisher/repository, persistent identifier, and publication year. Regarding the publisher/repository, please add "[data set]" or "[code]" to the entry (e.g., Zenodo [code]).
TS25   Andrews and Mahaffy (1976) is not mentioned in the text.
TS26   Please provide the complete author list.
TS27   Please provide the complete author list.
TS28   Please provide the volume and page range/article number.
TS29   Clark (1994) is not mentioned in the text.
TS30   Please provide the complete author list.
TS31   Please provide date of last access.
TS32   Please confirm.
TS33   Please provide the volume and page range/article number.
TS34   Deser et al. (2020) is not mentioned in the text.
TS35   Francis et al. (2017) is not mentioned in the text.
TS36   Please confirm addition of -UK.
TS37   Please provide the complete author list.
TS38   Hugonnet et al. (2021) is not mentioned in the text.

TS39 Please provide the complete author list.

TS40 Please provide the complete author list.

TS41 Locke and Locke (1991) is not mentioned in the text.

TS42 Please provide the volume.

TS43 Medrzycka et al. (2023) is not mentioned in the text.

TS44 Please provide the volume and page range/article number.

TS45 Please provide the complete author list.

TS46 Please provide the page range or article number.

TS47 Please provide the page range or article number.

TS48 Please confirm.

TS49 Please provide the complete author list.

TS50 Ramsey et al. (2012) is not mentioned in the text.

TS51 Please provide the page range or DOI.

TS52 Please provide the complete author list.

TS53 Please provide the page range or article number.

TS54 Serreze et al. (2009) is not mentioned in the text.

TS55 Please provide the complete author list.

TS56 Tepes et al. (2021) is not mentioned in the text.